Hepatitis E virus infection remodels the mature tRNAome in macrophages to orchestrate NLRP3 inflammasome response

Yunlong Li[a,b,1] (iD), Ruyi Zhang[b,1], Yining Wang[b], Pengfei Li[b], Yang Li[b], Harry L. A. Janssen[b,c], Robert A. de Man[b] (iD), Maikel P. Peppelenbosch[b] (iD), Xumin Ou[d,e,2] (iD), and Qiuwei Pan[b,2] (iD)

Hepatitis E virus (HEV) infection has been shown to activate NOD-like receptor family pyrin domain–containing 3 (NLRP3) inflammasome in macrophages, a key mechanism of causing pathological inflammation, but the mechanisms regulating this response remain poorly understood. Here, we report that the mature tRNAome dynamically responds to HEV infection in macrophages. This directs IL-1β expression, the hallmark of NLRP3 inflammasome activation, at mRNA and protein levels. Conversely, pharmacological inhibition of inflammasome activation abrogates HEV-provoked tRNAome remodeling, revealing a reciprocal interaction between the mature tRNAome and the NLRP3 inflammasome response. Remodeling the tRNAome results in improved decoding of codons directing leucine- and proline synthesis, which are the major amino acid constituents of IL-1β protein, whereas genetic or functional interference with tRNAome-mediated leucine decoding impairs inflammasome activation. Finally, we demonstrated that the mature tRNAome also actively responds to lipopolysaccharide (a key component of gram-negative bacteria)-triggered inflammasome activation, but the response dynamics and mode of actions are distinct from that induced by HEV infection. Our findings thus reveal the mature tRNAome as a previously unrecognized but essential mediator of host response to pathogens and represent a unique target for developing anti-inflammatory therapeutics.

hepatitis E virus | NLRP3 inflammasome | mature tRNAome | macrophages | amino acid deficiency

Hepatitis E virus (HEV) is the leading cause of acute viral hepatitis (1). Severe acute infection with massive liver inflammation resulting in high mortality rate has been widely reported in pregnant women. Such pathological inflammation is often driven by intense, rapid activation of the inflammasome pathway and release of pro-inflammatory mediators. The NOD-like receptor family pyrin domain–containing 3 (NLRP3) inflammasome is the best characterized form and most relevant to viral infections. NLRP3 inflammasome activation usually depends on two signals. Signal one is required for synthesis of pro-IL-1β and NLRP3 in a nuclear factor-κB (NF-κB)-dependent process. Signal two triggers assembly of the NLRP3 inflammasome complex, leading to the intracellular cleavage of pro-IL-1β and release of the mature IL-1β through caspase-1 autoactivation (2).

Monocytes and macrophages play essential roles in the inflammatory responses to pathogens including HEV (3). We have recently demonstrated that HEV is a robust activator of NLRP3 inflammasome in macrophages, revealing a potential mechanism of HEV-triggered hyperinflammation in patients (4). Thus, targeting NLRP3 inflammasome represents an innovative approach for therapeutic development of treating severe HEV infection, in addition to the classical antiviral treatment. However, this requires better understanding of underlying mechanisms of regulating HEV-triggered inflammasome response.

Current attention of understanding inflammatory response largely focuses on the transcriptional and translational landscapes, but translational decoding which bridges these two groups of processes has been largely ignored. Translational decoding is mediated by transfer RNAs (tRNAs). The human tRNAome is encoded by more than 600 tRNA gene loci. Following RNA polymerase III–mediated transcription, tRNAs are subjected to posttranscriptional modification, and a common CCA ribonucleotide sequence is added to the 3′ end to become the mature form. Mature tRNAs are typically 70 to 90 base pairs in length and charged with cognate amino acid, which is catalyzed by aminoacyl-tRNA synthetases (ARSs), providing the substrates for protein synthesis. Theoretically, the mature tRNAome shall contain 61 types of aminoacyl-tRNAs to decode the 61 triplet codons that specify the twenty primary amino acids in human proteins but the actual number of aminoacyl-tRNAs is smaller, wobbling and super wobbling being needed to explain

Significance

This study revealed the dynamics of the mature tRNAome landscape in response to pathogen-provoked inflammasome activation in macrophages. Mature tRNAs charge their corresponding amino acids for protein synthesis. Amino acid deprivation or knockdown of the enzyme responsible for tRNA charging demonstrated the functional implications in regulating inflammatory response. This study employed hepatitis E virus infection as a representative disease modality, but the relevance was also observed in lipopolysaccharide-activated inflammatory response, mimicking bacterial invasion. We postulate that tRNAome plays a ubiquitous role in orchestrating pathogen-induced inflammatory response and represent a unique target for developing anti-inflammatory therapeutics.

translation of all codons (5). Insight into the nature of the tRNAome in general and the mature tRNAome in particular is still largely in its infancy, mainly because of technical difficulties. Recently, we developed a technology that allows quantitative characterization of the entire mature human tRNAome (6), and we observed that HEV infection alters tRNAome composition (7), suggesting that alternative translational decoding may be involved in HEV-related pathology. Indeed, tRNA biogenesis and levels of ARSs are under the control of mTOR (8), and it is known that activity of the mTOR kinase is required for effective cell-autonomous immunity against HEV infection (9). More generally, accumulating evidence suggests that the composition of the tRNAome is a regulatory factor in immune regulation per se (10). In conjunction, these considerations prompt investigation in the potential role of tRNAome modulation in the activation of anti-HEV immune response.

In this study, we delineate how the host mature tRNAome orchestrates HEV-provoked inflammasome response and evaluate the potential of therapeutic targeting. We uncover the reciprocal interplay between the mature tRNAome and NLRP3 inflammasome response, providing unexpected unique insight into the mechanisms cells employ in reaction to HEV infection.

Results

Dynamic Coordination of IL-1β Transcription and Translation, and the Mature tRNAome Landscape upon HEV Infection in Macrophages. Our previous study has demonstrated that HEV can strongly activate NLRP3 inflammasome activation in differentiated human THP-1 macrophages. This was further confirmed in differentiated HL60 macrophage cell line, although to a much less extent (4). In this study, we first confirmed that inoculation of differentiated THP-1 and HL60 macrophages with infectious HEV particles resulted in active infection shown by increased levels of intracellular viral RNA (Fig. 1*A*), the presence of dsRNA (an intermediate of viral replication), and the expression of open reading frame 2 (ORF2) protein (*SI Appendix*, Fig. S1 *A–C*). Subsequently, we profiled the dynamics of IL-1β mRNA expression and protein secretion, a hallmark of inflammasome activation, upon HEV inoculation. Activation of IL-1β mRNA expression and secretion was observed in both THP-1 and HL60 macrophages, but the effect was much more profound in the THP-1 model, and thus THP-1 was used as the main model in this study (Fig. 1 *B* and *C*). Surprisingly, the kinetics of mRNA and protein expression was distinct. For example, the IL-1β mRNA level was
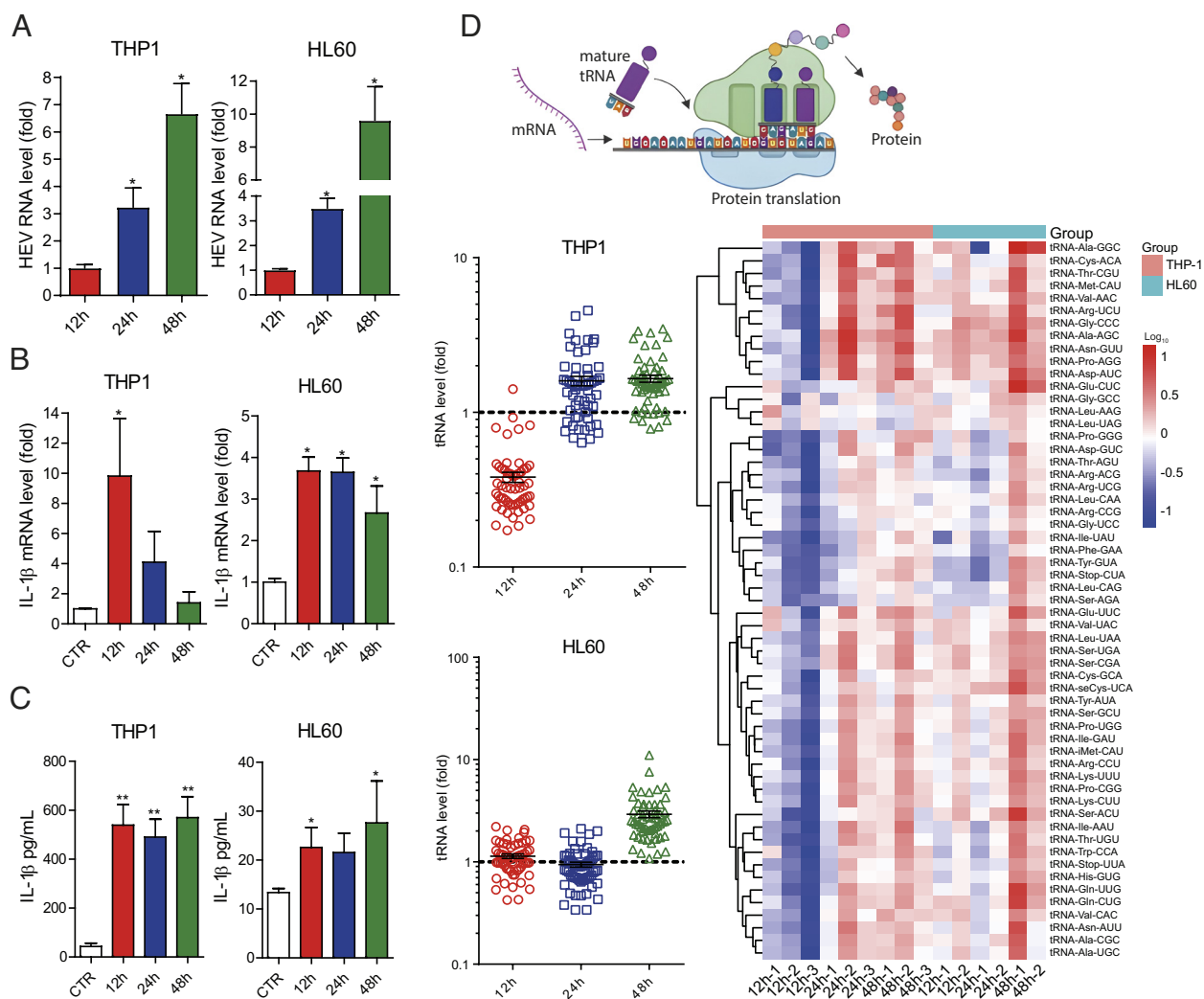
Fig. 1. The kinetics of IL-1β expression and the landscape of the mature tRNAome in macrophages upon HEV infection. (*A*) THP-1 and HL60 macrophages were inoculated with HEV particles and viral RNA levels were quantified by qRT-PCR (n = 4). IL-1β mRNA expression (n = 4) (*B*) and protein secretion (n = 6) (*C*) were quantified in THP-1 and HL60 macrophages after inoculation with HEV for 12, 24, or 48 h. (*D*) Accordingly, the mature tRNAome consisting of 57 species was quantified by qRT-PCR. Cluster analysis of the tRNAome and data were normalized to the control (CTR; set as 1). Data are means ± SEM. *P < 0.05; **P < 0.01.

the highest at 12 h postinoculation, and gradually decreased. However, the protein level of IL-1β quantified by enzyme-linked immunosorbent assay (ELISA) was stably maintained throughout the 48 h' course (Fig. 1 *B* and *C*).

This disparity in IL-1β mRNA and protein expression triggered our hypothesis that the landscapes of host tRNAome expression and processing may dynamically respond to and orchestrate HEV-provoked inflammasome response. Thus, we profiled the tRNAome consisting of 57 species of mature tRNAs by a specialized qRT-PCR method that we previously developed (10). Interestingly, the majority of tRNAs were down-regulated at 12 h postinoculation, but dramatically up-regulated at 24 and 48 h in the THP-1 model, and similar trend was also observed in HL60 (Fig. 1*D*). This is an inverse of the IL-1β mRNA expression pattern, which potentially explains why IL-1β protein expression can be stably sustained. Thus, these results appear to show a dynamic coordination of inflammatory gene transcription, translation, and the mature tRNAome landscape in response to HEV infection in macrophages.

Our previous study has shown that HEV genome per se does not trigger inflammasome response, but indirectly through the produced virus particles (4). Here, we assessed the effects of transfecting HEV genomic RNA into THP-1 macrophages and included the replication-defective genome (due to a GAD mutant). We found that delivery of the infectious HEV genome but not the GAD mutant resulted in viral replication (*SI Appendix,* Fig. S2*A*), IL-1β production (*SI Appendix,* Fig. S2*B*), and tRNAome remodeling (*SI Appendix,* Fig. S2*C*). However, since HEV particle is the potent and direct trigger of inflammasome response (4), we mainly employed inoculation of virus particles as the experimental approach in this study.

Inhibition of NLRP3 Inflammasome Prevents HEV-Triggered tRNAome Remodeling. Full activation of the NLRP3 inflammasome usually requires two signals. The initial signal induces the transcription of NLRP3 and pro-IL-1β through the activation of NF-κB pathway. The second signal of NLRP3 inflammasome activation leads to autoactivation of caspase-1, cleavage of pro-IL-1β, and secretion of mature IL-1β (11, 12). Consistently, we observed elevated levels of phosphorylated NF-κB p65 protein upon HEV inoculation (*SI Appendix,* Fig. S1*D*). Western blotting confirmed the increased level of pro-IL-1β and cleaved caspase-1 intracellularly, and the secretion of mature IL-1β in supernatant, upon HEV inoculation in THP-1 macrophages (Fig. 2*A*). This activation by HEV can be specifically blocked by treatment with BAY11-7085 (NF-κB inhibitor), MCC950 (NLRP3 inhibitor), or VX-765 (caspase-1 inhibitor) (Fig. 2 *B* and *C*). HEV remains capable of replicating in the presence of these inhibitors (Fig. 2*D*), and these inhibitors alone have minimal effects on the basal level of IL-1β secretion and cell viability (*SI Appendix,* Fig. S3 *A* and *B*). As expected, at a basal level without HEV infection, BAY11-7085 treatment also showed an inhibition of NLRP3 and pro-IL-1β protein expression (*SI Appendix,* Fig. S3*C*).

Importantly, HEV failed to reprogram the host mature tRNAome in the presence of these NLRP3 inflammasome inhibitors. The expression of the majority of mature tRNAs maintained around the basal levels from 12 to 48 h postinoculation (Fig. 2*E*). These results demonstrated that HEV-triggered tRNAome remodeling is a specific response to NLRP3 inflammasome activation.

Deprivation of Individual Amino Acid Affects HEV-Induced Inflammatory Gene Expression. Mature tRNAs charge cognate amino acids (forming aminoacyl-tRNAs) to catalyze protein synthesis. The availability of amino acids and the levels of corresponding mature tRNAs are intimately related. Thus, we investigated the functional implications of translational decoding on HEV-triggered inflammatory response by depriving individual amino acid in the culture medium of THP-1 macrophages. We employ an amino acid–free RPMI 1640 medium and supplement with the corresponding amino acid cocktail to deprive each one of the 20 amino acids. At the basal level without HEV infection, IL-1β production is very low in THP-1 macrophage, and amino acid deprivation has minimal effects on IL-1β secretion (*SI Appendix,* Fig. S4*A*) and cell viability (*SI Appendix,* Fig. S4*B*). In contrast, HEV infection activates the transcription of a panel of inflammatory response–related genes, including IL-1β, IL-6, IL-8, IL-12, Granulocyte-macrophage colony-stimulating factor (GM-CSF) and tumor necrosis factor alpha (TNF-α), in medium containing the 20 amino acids (Fig. 3*A*). Depleting each of them exerted variable effects on the transcription of these inflammatory genes, with somewhat an inhibitory effect in general (Fig. 3*B*). However, a universal inhibition of all these tested genes was observed by deprivation of leucine or proline (Fig. 3*B*). This is consistent with the results that most of the cognate tRNAs of leucine and proline are up-regulated upon HEV infection, in particular at 24- or 48-h postinoculation (Fig. 3*C*). Of note, leucine or proline deprivation did not affect HEV replication (*SI Appendix,* Fig. S5), indicating the specificity on HEV-induced inflammatory gene expression.

Leucine or Proline Deprivation Abolished HEV-Induced Inflammasome and tRNAome Reprogramming. Given the prominent role of leucine and proline in HEV-activated inflammatory gene expression (Fig. 3*B*), we next investigated the effects of leucine or proline deprivation on HEV-induced NLRP3 inflammasome response. We found that depleting leucine or proline largely blocks IL-1β production in THP-1 macrophages inoculated with HEV (Fig. 4*A*). HEV activates the production of cleaved caspase-1 and cleaved IL-1β, the hallmarks of NLRP3 inflammasome full activation, but their production was almost completely blocked by leucine or proline deprivation (Fig. 4*B*). Accordingly, HEV-provoked tRNAome remodeling in the control group without amino acid deprivation (*SI Appendix,* Fig. S6), whereas depleting leucine or proline largely attenuated HEV-triggered tRNAome remodeling (Fig. 4*C*). Furthermore, leucine or proline deprivation did not affect the IL-1β secretion (*SI Appendix,* Fig. S7*A*) and mature tRNAome expression (*SI Appendix,* Fig. S7*B*) in THP-1 macrophages without HEV infection, indicating the specificity on HEV-induced inflammasome and tRNAome reprogramming.

Since amino acids are charged with mature tRNAs that supply the charged amino acid to protein synthesis, the availability of different aminoacyl-tRNA species that fit codon usage and amino acid composition of a given gene is expected to effectively produce the protein (13). Because IL-1β is abundantly secreted during NLRP3 inflammasome activation by HEV infection, we performed a need-to-supply analysis based on codon usage and amino acid composition between IL-1β gene and the mature tRNAome landscape. Interestingly, we found that leucine is the most abundant amino acid within the IL-1β protein (*SI Appendix,* Fig. S8*A*). According to the IL-1β mRNA coding sequence, the Leu-CUG codon frequently occurs which cognates with its anticodon-changed tRNA, tRNA-Leu-CAG (*SI Appendix,* Fig. S8*B*). By performing relative synonymous codon usage (RSCU) analysis (14), a highly used tRNA-Leu-CAG was identified, for example, reaching 3 (*SI Appendix,* Fig. S8*C*). Importantly, leucine (green) is predominately located at the beta-sheet of IL-1β protein, in particular of the secreted form. However, proline (red) is mainly located at multiple turn regions (*SI Appendix,* Fig. S8*D*). Thus, we further studied the functional implications of the biological process of leucine-tRNA charging.
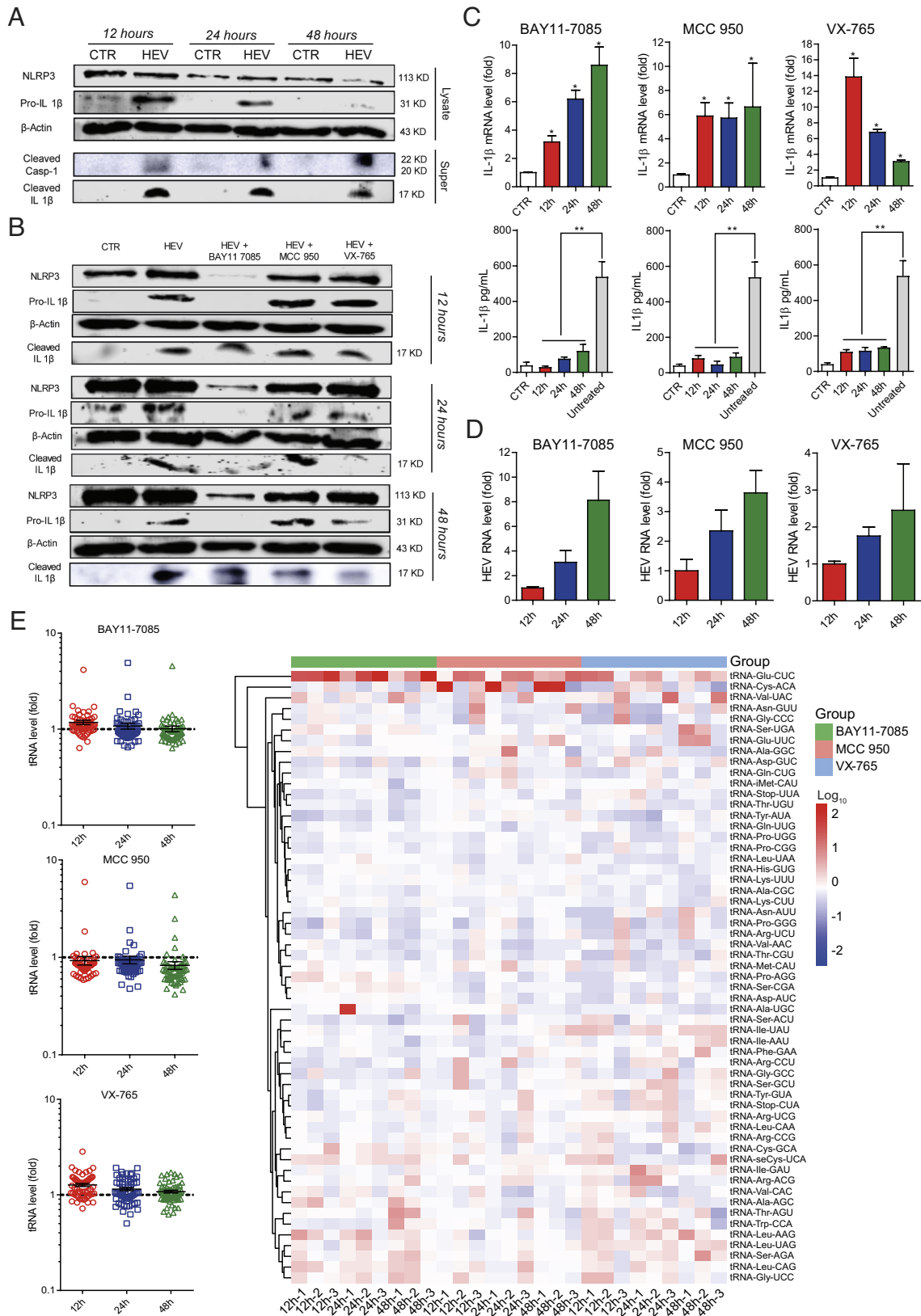
Fig. 2. Inhibition of NLRP3 inflammasome prevents HEV-induced tRNAome reprogramming. (*A*) THP-1 macrophages were inoculated with HEV for 12, 24, or 48 h. Mature IL-1β and cleaved caspase-1 in supernatant or pro-IL-1β and NLRP3 in lysates were determined by western blotting. THP-1 macrophages were pretreated with 10 μM NF-κB inhibitor (BAY11-7085), 10 μM NLRP3 inhibitor (MCC950), or 50 μM caspase-1 inhibitor (VX-765) for 2 h and then were incubated with HEV or HEV plus 10 μM BAY11-7085, 10 μM MCC950, or 50 μM of VX-765 for 12, 24, or 48 h. (*B*) Mature IL-1β in supernatant or pro-IL-1β and NLRP3 in lysates were determined by western blotting. (*C*) IL-1β mRNA and protein levels were quantified by qRT-PCR (n = 4 to 5) and ELISA (n = 4 to 6), respectively. (*D*) HEV mRNA levels were quantified by qRT-PCR (n = 3 to 5). (*E*) The mature tRNAome was quantified by qRT-PCR. Cluster analysis of the tRNAome and data were normalized to the control (CTR; set as 1). Data are means ± SEM. *P < 0.05; **P < 0.01.
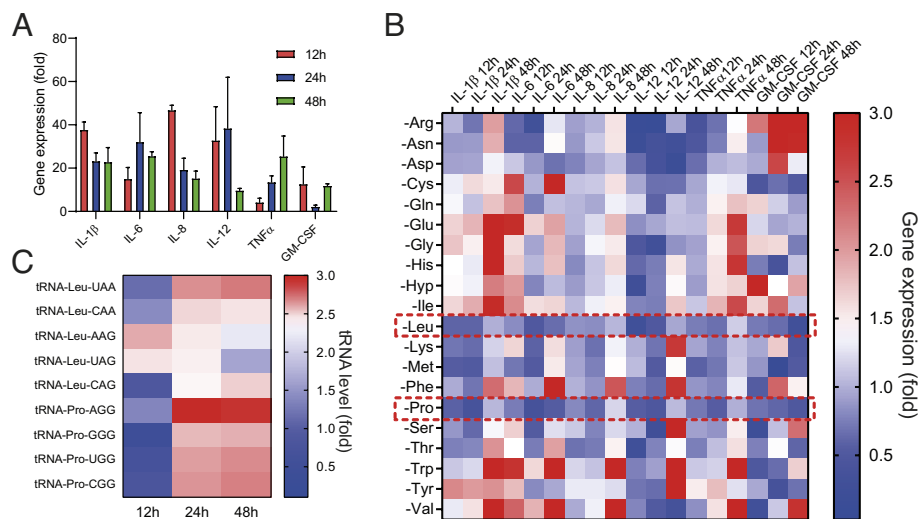
Fig. 3. Amino acid deprivation affects HEV-induced inflammatory gene expression. (*A*) THP-1 macrophages were cultured in medium containing 20 amino acids and inoculated with HEV for 12, 24, or 48 h. Gene expression of IL-1β, IL-6, IL-8, IL-12, TNFα, or GM-CSF was quantified by qRT-PCR (n = 3). (*B*) THP-1 macrophages were subjected to the deprivation of each of the 20 amino acids in RPMI 1640 and inoculated with HEV for 12, 24, or 48 h. The expression of inflammatory genes was quantified by qRT-PCR (n = 3), and data were normalized to the nonamino acid deprivation group (set as 1). (*C*) THP-1 macrophages were inoculated with HEV for 12, 24, or 48 h. The cognate tRNAs of leucine and proline were quantified by qRT-PCR, and data were normalized to the uninfected group (set as 1).

Knockdown of Leucyl-tRNA-Synthetase Attenuates HEV-Induced Inflammatory Response. ARSs are the enzymes charging mature tRNAs with their cognate amino acids. Leucyl-tRNA synthetase (LRS), encoded by LARS, catalyzes the charging of leucine to its cognate mature tRNA (Fig. 5*A*). Since LARS has key biological functions, we expect that complete loss of LARS would profoundly affect cellular physiology. Thus, to investigate the function of LRS, we used lentiviral RNAi to stably down-regulate LARS expression in THP-1 macrophages, and a vector without targeting any host genes (shCTR) served as a negative control. We selected an shRNA with optimal efficiency of gene knockdown based on mRNA expression (Fig. 5*B*). At a basal level without HEV infection, LARS knockdown and control cells had a similar level of mature IL-1β secretion (*SI Appendix*, Fig. S9*A*) and tRNAome landscape (*SI Appendix*, Fig. S9*B*). When cells inoculated with HEV, the induction of inflammatory gene expression was dramatically attenuated in LARS knockdown compared to the control cells (Fig. 5*C*). Consistently, HEV-triggered secretion of IL-1β (Fig. 5*D*) and the levels of NLRP3, pro-IL-1β, cleaved caspase-1, and IL-1β (Fig. 5*E*) were also attenuated in LARS knockdown macrophages, although not a complete abolishment. Finally, HEV failed to effectively remodel the host tRNAome in LARS knockdown cells (Fig. 5*F*). Taken together, the dynamics of mature tRNAome landscape and the process of charging corresponding amino acids play essential role in orchestrating HEV-triggered NLRP3 inflammasome response.

A Broad Implication of tRNAome in Regulating Inflammatory Response. Lipopolysaccharide (LPS) is a key component of the outer membrane of gram-negative bacteria, acting as a natural activator of inflammasome/inflammatory responses (15). As expected, simulating bacterial invasion by adding LPS plus Adenosine 5'-triphosphate (ATP) strongly activates inflammasome response in macrophages (*SI Appendix*, Figs. S10 *A and B* and S11 *A and B*). This is accompanied by the dramatic reprogramming of the mature tRNAome (*SI Appendix*, Fig. S10*C*). Pharmacological inhibitors potently inhibit inflammasome activation and the remodeling of tRNAome (*SI Appendix*, Fig. S11 *C and D*). Amino acid deprivation assay found that depleting arginine

effectively inhibited LPS-triggered inflammatory gene expression (*SI Appendix*, Fig. S12*B*). Consistently, the cognate tRNAs of arginine were all highly up-regulated at 12 h after LPS treatment (*SI Appendix*, Fig. S12*C*). By performing RSCU analysis (14), a high ratio of tRNA-Arg-UCG was found, for example, reaching 3 (*SI Appendix*, Fig. S12*D*). These results demonstrated that the mature tRNAome actively orchestrates LPS-induced inflammatory response, but the dynamics of tRNAome response and mode of actions are distinct from that triggered by HEV infection.

Discussion

Mature tRNAs perform central functions in protein synthesis by charging with cognate amino acids, decoding mRNA codons, and elongating peptides. Dysregulation of tRNA expression, processing, and modification is associated with a variety of diseases, including cancer, diabetes mellitus, and neuronal disorders (16–20). Viruses solely rely on the host cell translation machinery to synthesize viral proteins (21). Segmented studies have indicated emerging roles of host tRNAome in responding and regulating viral infections (22). For example, it has been shown that tRNA$^{Arg(UCU)}$ and tRNA$^{Ile(UAU)}$ are the most overrepresented species in influenza A viruses and vaccinia virus–infected cells, respectively, to favor the translation of viral proteins (23). Our team has previously shown that HEV infection dramatically reprograms the mature tRNAome in liver cells, which is expected to facilitate the translation of viral proteins in particular the capsid protein (6, 7). In this study, we demonstrated a prominent role of the mature tRNAome in orchestrating HEV-triggered NLRP3 inflammasome activation in macrophages.

Acute HEV infection in vulnerable populations such as pregnant women can cause severe liver inflammation, accompanied by high levels of pro-inflammatory cytokines such as TNF-α, IL-6, interferon-gamma (IFN-γ), IL-18, and IL-1β (24, 25). Monocytes and macrophages, the key immune cell types driving pathological inflammation, are permissive to HEV infection (26). The frequencies of monocytes and macrophages are increased in HEV-infected pregnant women (27). We recently found that HEV infection robustly activates NLRP3 inflammasome activation in macrophages,
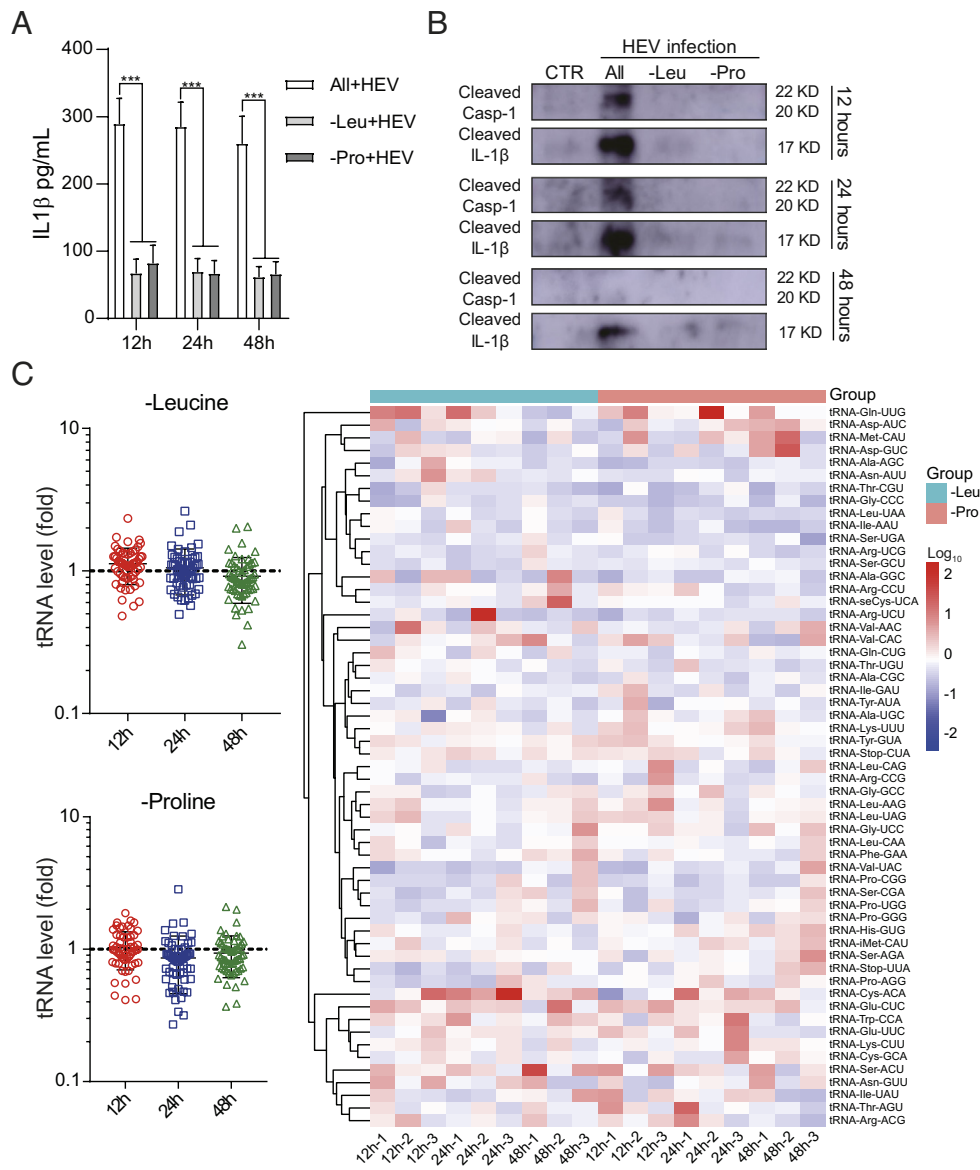
Fig. 4. Leucine or proline deprivation abolishes HEV-induced inflammasome activation and tRNA reprogramming. THP-1 macrophages were subjected to 20 amino acid–containing, leucine deprivation, or proline deprivation RPMI 1640 medium and inoculated with HEV for 12, 24, or 48 h. (*A*) IL-1β protein levels were quantified by ELISA (n = 10 to 12). (*B*) Mature IL-1β and cleaved caspase-1 in the supernatant were determined by western blotting. (*C*) The mature tRNAome was quantified by qRT-PCR. Cluster analysis of the tRNAome and data were normalized to the control (CTR; set as 1). Data are means ± SEM. *P < 0.05; **P < 0.01; ***P < 0.001.

revealing a key mechanism of HEV-triggered inflammatory response (4). Since the THP-1 macrophage is an excellent model for studying HEV-induced inflammatory activation, which is much more sensitive in responding to inflammatory triggers for example in comparison to HL60 macrophages (4), it is thus used as the main model in the current study. Here, we found that the landscape of mature tRNAome dynamically responded to HEV infection in macrophages. Most of the tRNA species were up-regulated at 24- and 48-h postinoculation. In contrast, the expression of IL-1β mRNA was rapidly increased at 12 h but sharply declined at 24 and 48 h, whereas the expression of IL-1β protein was maintained throughout the 2-d period (Fig. 1). IL-1β has a very short half-life in plasma in vivo. For example, the half-life of recombinant human IL-1β in rats ranged from 19 min to 1.59 h (28). Consistently, the intracellular form of pro-IL-1β in LPS-stimulated THP-1 monocytes and primary monocytes has a short half-life of 2.5 h. Mechanistically, proteasome mediates

the rapid degradation of IL-1β in macrophages (29). Thus, the maintained level of IL-1β in our model is not related to the stability of pro-IL-1β or mature IL-1β, but reflects the coordination of transcription, translation, and translational decoding during inflammatory response.

Treatment with pharmacological inhibitors of inflammasome activation completely prevented HEV-triggered tRNAome remodeling (Fig. 2), supporting the specificity of this response. However, the mechanism of how mature tRNAome is up-regulated during inflammasome activation remains unknown. We postulate that this may occur at tRNA transcription or the process of maturation, but requires further investigation. Surprisingly, the majority of mature tRNAs were down-regulated at 12 h postinoculation (Fig. 1). We speculate this may serve as a protective mechanism of preventing overactivation immediately upon HEV invasion. Such rapid down-regulation of mature tRNAs may be exerted by tRNA fragmentation, rather than inhibition of tRNA transcription. Notably, levels
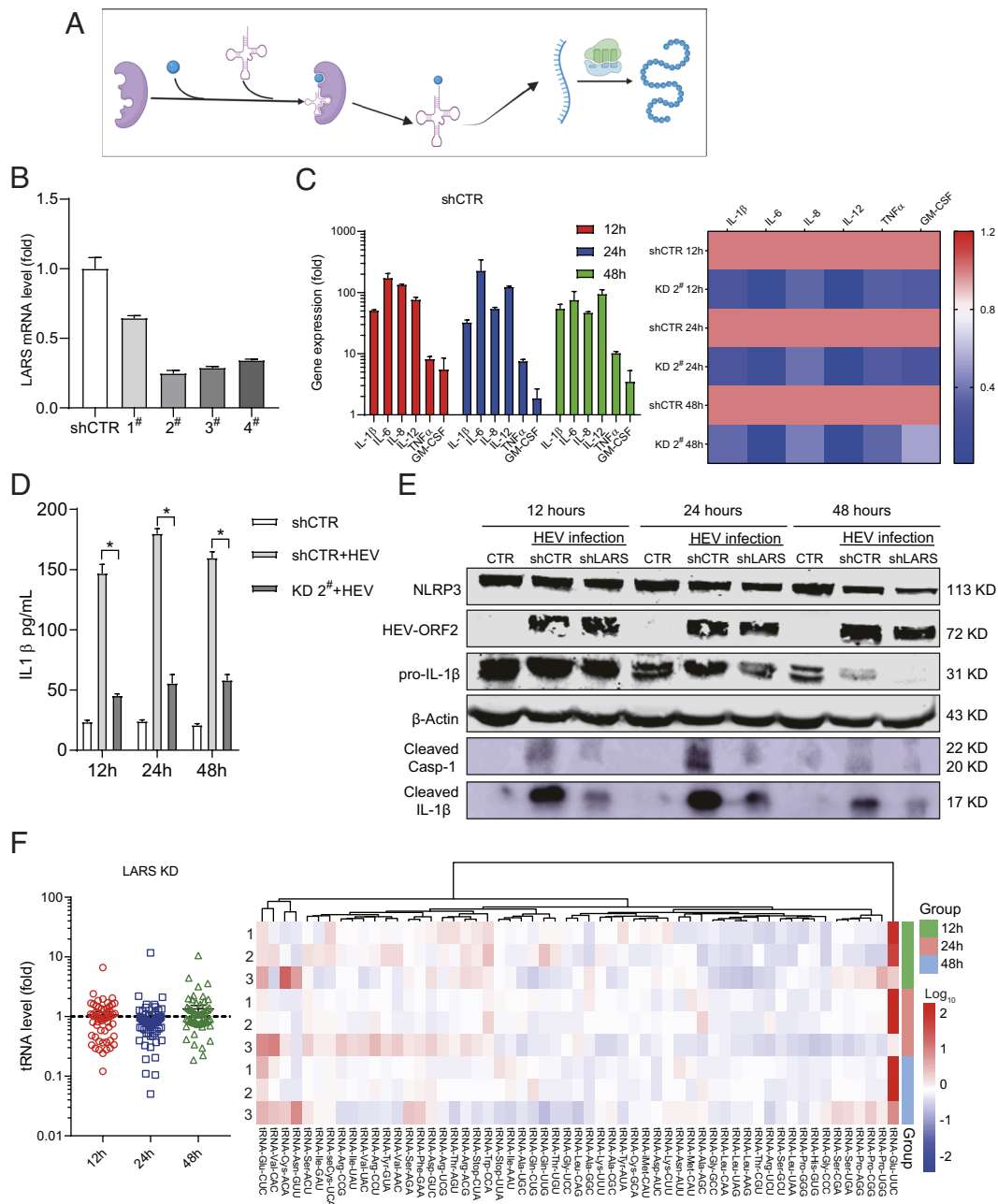
Fig. 5. Knockdown of leucyl-tRNA-synthetase attenuates HEV-induced inflammatory response and tRNA reprogramming. (*A*) Schematic illustration of the process of aminoacylated tRNAs biogenesis. (*B*) LARS mRNA expression of THP-1 cells following shRNA mediated knockdown was quantified by qRT-PCR, and the shCTR control (cells transduced with a vector without targeting any host genes) was set as 1. Effects of LARS knockdown on inflammasome response measured after inoculation with HEV for 12, 24, or 48 h. (*C*) The expression levels of inflammatory genes were quantified by qRT-PCR (n = 4). (*D*) IL-1β protein levels were quantified by ELISA (n = 4). (*E*) Mature IL-1β and cleaved caspase-1 in the supernatant, and NLRP3, HEV ORF2, and pro-IL-1β in lysates were determined by western blotting. (*F*) The mature tRNAome was quantified by qRT-PCR. Cluster analysis of the tRNAome and data were normalized to the control (CTR; set as 1). Data are means ± SEM. *P < 0.05.

of circulating tRNA fragments in humans and animal models are sensitive to various pathophysiological conditions, such as acute inflammation and tissue damage (30).

Mature tRNAs are charged with the corresponding amino acids for conducting protein synthesis. The availabilities of both individual amino acids and the cognate tRNAs are expected to be limiting factors for protein synthesis. By selectively depriving each of the 20 amino acids, we identified that leucine or proline deprivation completely abolished HEV-induced inflammasome response and tRNAome reprogramming (Figs. 3 and 4), which is independent of the level of viral replication. Consistently, the cognate tRNAs of leucine and proline are universally up-regulated

at 24- and 48-h postinfection (Fig. 3C). Technically, we employed the group without amino acid deprivation as a control when assessing the impact of depriving leucine or proline, which is a common approach in designing such experimentation (e.g., in the field of cancer research) (31). Since each amino acid may have its specific functions, it is uncertain whether depleting any other amino acid could serve as an appropriate control. Nevertheless, the effects of depleting other amino acids could be interesting to be further studied, although in this study, we only focused on leucine and proline which showed the most prominent effects.

ARSs catalyze the aminoacylation reaction by linking amino acids to their cognate tRNAs. We used lentiviral shRNA vectors

to stably knock down LARS, the enzyme charging leucine to its cognate tRNAs. We found that downregulation of LARS effectively inhibited HEV-triggered NLRP3 inflammasome activation and tRNAome reprogramming (Fig. 5). However, the inhibitory effect was slightly lower compared to that seen in leucine deprivation. This is probably explained by the partial knockdown of LARS expression. Because it is an essential enzyme required for maintaining cellular physiology, complete knockout is likely detrimental to cell survival.

Inflammation is a ubiquitous response to tissue injuries and pathogen invasions. We thus extended our investigation by profiling tRNAome in macrophages stimulated with LPS, a natural activator of inflammasome produced by gram-negative bacteria (15). We also observed the remodeling of tRNAome and demonstrated the functional relevance by pharmacological inhibitors of inflammasome activation and amino acid deprivation (*SI Appendix,* Figs. S10–S12). However, the dynamics of tRNAome remodeling and the specific amino acids identified in regulating inflammatory response are distinct from those observed in the setting of HEV infection (Fig. 3 and *SI Appendix,* Fig. S12). This suggests that tRNAome may universally orchestrate inflammatory response, but the exact mode of actions are likely pathogen- and context-dependent. The roles of tRNAs in regulating pathogen–host interactions likely go far beyond inflammatory response, involving in both innate and adaptive immunity (10, 32).

The critical roles of tRNAome in the pathophysiology of various diseases in turn provide unique targets for therapeutic development. Amino acid deprivation based on dietary modulation or pharmacological targeting of specific enzymes has been explored for treating cancer and viral infections (33–38). Pharmacological inhibitors of ARSs have been developed for treating bacterial or parasite infections. Because of the species specificity, these agents are designed to preferentially target pathogen but not human ARSs to minimize side effects (35). A very recent study demonstrated the use of recombinant adeno-associated virus vector–based delivery of nonsense suppressor tRNAs to rescue pathogenic nonsense mutations, and restore gene function in a mouse model of a genetic disease (39). In this study, we demonstrated the feasibility of inhibiting pathogen-triggered inflammatory response through amino acid deprivation and ARS inhibition. These results support the notion that targeting the biological process of amino acid and cognate tRNA charging can be explored for antiinflammation treatment (e.g., amino acid–defined nutrition recipes), but the exact targets and therapeutic modalities require further research.

In summary, this study mapped the dynamics of the mature tRNAome landscape in response to HEV-triggered NLRP3 inflammasome activation. Further investigation demonstrated the specificity and functional implications of tRNAome in regulating inflammatory response. A similar phenomenon was observed in LPS-triggered inflammasome activation. Thus, this likely represents a universal mechanism in orchestrating pathogen–host interactions, going beyond HEV infection and inflammation. Hopefully, these findings will open up perspectives in studying the pathophysiology of HEV infection and developing unique therapeutics.

Materials and Methods

Reagents. Reagents used in this study including antibodies, chemicals, and kits are listed in *SI Appendix,* Table S1.

Cell Culture. Human monocytic cell lines (THP-1 and HL60) were cultured in Roswell Park Memorial Institute (RPMI) 1640 medium (ThermoFisherScientific), complemented with 10% (v/v) inactivated fetal bovine serum (FBS) with 100 IU/mL of penicillin and 100 mg/mL of streptomycin. For macrophage differentiation, THP-1 and HL60 cells were treated with 15 and 40 ng/mL of phorbol 12-myristate

13-acetate (PMA) at 37 °C for 48 h, respectively. Then, cells were cultured for another 24 h without PMA. Human hepatoma cell line (Huh7) and human embryonic kidney epithelial cell line (293T) were cultured in Dulbecco's Modified Eagle Medium supplemented with 10% FBS, 100 IU/mL penicillin, and 100 mg/mL streptomycin. All cells were maintained at 37 °C in a 5% CO2 atmosphere. Cell line authentication was performed using the short tandem repeat genotyping assay at the Molecular Diagnostics Department, Erasmus Medical Center. The mycoplasma-free status was regularly (commercially) checked and confirmed based on the real-time PCR method at Eurofins GATC-Biotech.

Production of Infectious HEV in Cell Culture. Plasmid constructs containing the full-length HEV genome (Kernow-C1 p6 clone; GenBank Accession Number JQ679013) and HEV replication–defective replicon (the GDD motif mutated to GAD) were transcribed into genomic RNA in vitro from corresponding enzyme-digested and linearized plasmid DNA using Ambion mMESSAGE nMACHINE T7 RNA kits (Invitrogen) (40). For producing HEV particles, Kernow-C1 p6 full-length genomic RNA was delivered into Huh7 cells by electroporation. Infectious HEV particles were collected from these Huh7 cells by freeze-thawing three times and harvested by centrifugation at 4,000 rpm for 10 min to remove cell debris and then ultracentrifugation at 22,000 rpm for 2 h to pellet the virus (SW 28 rotor). The pellet was suspended with RPMI 1640 or 1640 without amino acid, then copy numbers were quantified as previously described (7) and diluted to 1×10^7 HEV viral RNA copies/mL. This virus stock was stored at −80 °C.

HEV Inoculation. The stored virus stock was used for inoculation. In brief, for the initial infection assay, 1.5×10^5 THP-1 or HL60 cells per well were seeded into 48-well plates and differentiated into macrophages. These differentiated macrophages were incubated with 200 μL of the HEV stock (1×10^7 HEV viral RNA copies/mL). After 12, 24, or 48 h of incubation, supernatant and cells were collected for quantifying IL-1β protein, HEV RNA, and or inflammatory gene expression, respectively. For the subsequent experimentations, 2.5×10^5 cells per well were seeded into 24-well plates and inoculated with 300 μL virus stock for quantifying tRNAome and characterizing inflammasome response. For MTT (3-[4,5-dimethylthiazol-2-yl]-2,5 diphenyl tetrazolium bromide) assay, 5×10^4 cells per well were seeded into 96-well plates and inoculated with 75 μL virus stock. For western blotting, 1×10^6 cells per well were seeded into six-well plates and inoculated with 1 mL HEV stock.

RNA Isolation and qRT-PCR. RNA was isolated by the NucleoSpin® RNA isolation kit of Macherey-Nagel (Bioke), quantified by NanoDrop ND-1000 (Wilmington, DE, USA), and reverse-transcribed into cDNA using the PrimeScript™ RT Master Mix (Perfect Real Time, Takara, cat# RR036A), according to the manufacturer's instructions. RNA expression levels were quantified by SYBR Green–based qRT-PCR (Applied Biosystems SYBR Green PCR Master Mix; Thermo Fisher Scientific Life Sciences) with the StepOnePlus System (Thermo Fisher Scientific Life Sciences). Glyceraldehyde 3-phosphate dehydrogenase was used as a reference gene to normalize target gene expression using the formula $2^{-\Delta\Delta CT}$ ($\Delta\Delta CT = \Delta CTsample - \Delta CTcontrol$). The genes primers are listed in *SI Appendix,* Table S2. For tRNA quantification, we used the isolation protocol and primer sequences that we previously described (6).

Amino Acid Deprivation Assay. Human monocytic cell line THP-1 was treated with 15 ng/mL of PMA at 37 °C for 48 h. Then, cells were cultured for another 24 h without PMA. Subsequently, cells were washed three times with 1 × PBS and then cultured in RPMI 1640 medium without amino acids (RPL22, Caisson Labs) for 24 h to establish an amino acid deprivation model. To further test the deprivation of each of the 20 amino acids, different amino acids except for the deprived one were then added, according to the concentrations of amino acids in regular complete RPMI 1640 medium (31, 33). Adding culture medium containing all 20 amino acids (without deprivation) served as control.

Lentiviral shRNA Packaging and Transduction. To perform gene knockdown, pLKO.1-based lentiviral vectors (Sigma-Aldrich) targeting LARS and a scrambled control vector (shCTR) were obtained from the Erasmus Medical Center for Biomics. These shRNA sequences are listed in *SI Appendix,* Table S3. Lentiviral pseudoparticles were generated in HEK293T cells. After 2 d of transfection with the lentiviral particles, THP1 cells were subsequently selected by 5 μg/mL puromycin (Sigma-Aldrich) for 1 to 2 wk until resistant clones appeared (41). The knockdown efficiency was confirmed by qRT-PCR. The target sequences of selected primers

were as follows: LARS sense 5'-CGTCGTTCCTTCATCACCACTG-3'; LARS anti sense 5'- AGGCTGTCCATCTTTCGGAGAG-3'.

Statistical Analysis. Statistical analysis was performed using the nonpaired, non-parametric test (Mann–Whitney *U* test; GraphPad Prism software, GraphPad Software Inc.). All results were presented as mean ± SEM. *P* values <0.05 (single asterisks in figures) were considered statistically significant, whereas *P* values <0.01 (double asterisks) and 0.001 (triple asterisks) were considered highly significant.

Additional description of methodology can be found in *SI Appendix, Materials and Methods*.

Data, Materials, and Software Availability. All the original data of this study have been deposited in Data Archiving and Networked Services, and are publicly available (https://doi.org/10.17026/dans-zyb-9pcv) (42).

Author affiliations: [a]Medical Faculty, Kunming University of Science and Technology, 450500 Kunming, Yunnan, China; [b]Department of Gastroenterology and Hepatology, Erasmus MC-University Medical Center, 3015GD Rotterdam, The Netherlands; [c]Toronto Centre for Liver Disease, Toronto General Hospital, Toronto, M5G 2C4 ON, Canada; [d]Engineering Research Center of Southwest Animal Disease Prevention and Control Technology, Ministry of Education of the People's Republic of China, 611130 Chengdu, Sichuan, China; and [e]Key Laboratory of Animal Disease and Human Health of Sichuan Province, Sichuan Agricultural University, Wenjiang, 611830 Chengdu, Sichuan, China

1. J. H. Hoofnagle, K. E. Nelson, R. H. Purcell, Hepatitis E. *N. Engl. J. Med.* **367**, 1237–1244 (2012).
2. C. Zhao, W. Zhao, NLRP3 inflammasome-A key player in antiviral responses. *Front Immunol.* **11**, 211 (2020).
3. J. M. Zhang, J. An, Cytokines, inflammation, and pain. *Int. Anesthesiol. Clinics* **45**, 27–37 (2007).
4. Y. Li *et al.*, Hepatitis E virus infection activates NOD-like receptor family pyrin domain-containing 3 inflammasome antagonizing interferon response but therapeutically targetable. *Hepatology (Baltimore, Md.)* **75**, 196–212 (2022).
5. X. Ou, J. Cao, A. Cheng, M. P. Peppelenbosch, Q. Pan, Errors in translational decoding: tRNA wobbling or misincorporation? *PLoS Genet.* **15**, e1008017 (2019).
6. X. Ou *et al.*, A simplified qPCR method revealing tRNAome remodeling upon infection by genotype 3 hepatitis E virus. *FEBS Lett.* **594**, 2005–2015 (2020).
7. P. Li *et al.*, Recapitulating hepatitis E virus-host interactions and facilitating antiviral drug discovery in human liver-derived organoids. *Sci. Adv.* **8**, eabj5908 (2022).
8. J. Guillon *et al.*, tRNA biogenesis and specific aminoacyl-tRNA synthetases regulate senescence stability under the control of mTOR. *PLoS Genet.* **17**, e1009953 (2021).
9. X. Zhou *et al.*, Rapamycin and everolimus facilitate hepatitis E virus replication: Revealing a basal defense mechanism of PI3K-PKB-mTOR pathway. *J. Hepatol.* **61**, 746–754 (2014).
10. C. Zhu, B. Sun, A. Nie, Z. Zhou, The tRNA-associated dysregulation in immune responses and immune diseases. *Acta Physiol. (Oxford, England)* **228**, e13391 (2020).
11. S. K. Vanaja, V. A. Rathinam, K. A. Fitzgerald, Mechanisms of inflammasome activation: Recent advances and novel insights. *Trends Cell Biol.* **25**, 308–315 (2015).
12. R. C. Coll, L. O'Neill, K. Schroder, Questions and controversies in innate immune research: What is the physiological role of NLRP3? *Cell Death Discov.* **2**, 16019 (2016).
13. N. N. Pavlova *et al.*, Translation in amino-acid-poor environments is limited by tRNA(Gln) charging. *Elife* **9**, e62307 (2020).
14. D. Paulet, A. David, E. Rivals, Ribo-seq enlightens codon usage bias. *DNA Res.* **24**, 210–303 (2017).
15. P. Yu, Y. Li, Y. Wang, M. P. Peppelenbosch, Q. Pan, Lipopolysaccharide restricts murine norovirus infection in macrophages mainly through NF-κB and JAK-STAT signaling pathway. *Virology* **546**, 109–121 (2020).
16. S. O. Sulima, I. J. F. Hofman, K. De Keersmaecker, J. D. Dinman, How ribosomes translate cancer. *Cancer Discov.* **7**, 1069–1087 (2017).
17. M. Santos, A. Fidalgo, A. S. Varanda, C. Oliveira, M. A. S. Santos, tRNA deregulation and its consequences in cancer. *Trends Mol. Med.* **25**, 853–865 (2019).
18. S. Q. Huang *et al.*, The dysregulation of tRNAs and tRNA derivatives in cancer. *J. Exp. Clin. Cancer Res. CR* **37**, 101 (2018).
19. Z. Zhou, B. Sun, S. Huang, W. Jia, D. Yu, The tRNA-associated dysregulation in diabetes mellitus. *Metab. Clin. Exp.* **94**, 9–17 (2019).
20. F. Tuorto, R. Parlato, rRNA and tRNA bridges to neuronal homeostasis in health and disease. *J. Mol. Biol.* **431**, 1763–1779 (2019).
21. M. Marques, B. Ramos, A. R. Soares, D. Ribeiro, Cellular proteostasis during influenza A virus infection-friend or foe? *Cells* **8**, 228 (2019).
22. A. Nunes *et al.*, Emerging roles of tRNAs in RNA virus infections. *Trends Biochem. Sci.* **45**, 794–805 (2020).
23. M. Pavon-Eternod *et al.*, Vaccinia and influenza A viruses select rather than adjust tRNAs to optimize translation. *Nucleic Acids Res.* **41**, 1914–1921 (2013).
24. S. G. Devi, A. Kumar, P. Kar, S. A. Husain, S. Sharma, Association of pregnancy outcome with cytokine gene polymorphisms in HEV infection during pregnancy. *J. Med. Virol.* **86**, 1366–1376 (2014).
25. V. Thakur, R. K. Ratho, M. P. Singh, Y. Chawla, S. Taneja, NLRP3 inflammasome activation is a prognostic marker of recovery in HEV-infected patients. *Curr. Microbiol.* **79**, 44 (2022).
26. I. M. Sayed *et al.*, Replication of hepatitis E virus (HEV) in primary human-derived monocytes and macrophages in vitro. *Vaccines* **8**, 239 (2020).
27. R. Sehgal *et al.*, Impaired monocyte-macrophage functions and defective Toll-like receptor signaling in hepatitis E virus-infected pregnant women with acute liver failure. *Hepatology (Baltimore, Md.)* **62**, 1683–1696 (2015).
28. S. Kudo, K. Mizuno, Y. Hirai, T. Shimizu, Clearance and tissue distribution of recombinant human interleukin 1 beta in rats. *Cancer Res.* **50**, 5751–5755 (1990).
29. M. A. Moors, S. B. Mizel, Proteasome-mediated regulation of interleukin-1beta turnover and export in human monocytes. *J. Leukocyte Biol.* **68**, 131–136 (2000).
30. P. Schimmel, The emerging complexity of the tRNA world: Mammalian tRNAs beyond protein synthesis. *Nat. Rev. Mol. Cell Biol.* **19**, 45–58 (2018).
31. X. Tang *et al.*, Cystine deprivation triggers programmed necrosis in VHL-deficient renal cell carcinomas. *Cancer Res.* **76**, 1892–1903 (2016).
32. N. Netzer *et al.*, Innate immune and chemically triggered oxidative stress modifies translational fidelity. *Nature* **462**, 522–526 (2009).
33. R. Zhang *et al.*, The biological process of lysine-tRNA charging is therapeutically targetable in liver cancer. *Liver Int. off. J. Int. Assoc. Study Liver* **41**, 206–219 (2021).
34. H. S. Fernandes, C. S. Silva Teixeira, P. A. Fernandes, M. J. Ramos, N. M. Cerqueira, Amino acid deprivation using enzymes as a targeted therapy for cancer and viral infections. *Expert Opin. Therap. Patents* **27**, 283–297 (2017).
35. S. C. Xie *et al.*, Reaction hijacking of tyrosine tRNA synthetase as a new whole-of-life-cycle antimalarial strategy. *Science (New York, N.Y.)* **376**, 1074–1079 (2022).
36. R. Missiaen *et al.*, GCN2 inhibition sensitizes arginine-deprived hepatocellular carcinoma cells to senolytic treatment. *Cell Metab.* **34**, 1151–1167.e1157 (2022).
37. F. Xiao *et al.*, Leucine deprivation increases hepatic insulin sensitivity via GCN2/mTOR/S6K1 and AMPK pathways. *Diabetes* **60**, 746–756 (2011).
38. L. Feun *et al.*, Arginine deprivation as a targeted therapy for cancer. *Curr. Pharm Des.* **14**, 1049–1057 (2008).
39. J. Wang *et al.*, AAV-delivered suppressor tRNA overcomes a nonsense mutation in mice. *Nature* **604**, 343–348 (2022).
40. P. Shukla *et al.*, Adaptation of a genotype 3 hepatitis E virus to efficient growth in cell culture depends on an inserted human gene segment acquired by recombination. *J. Virol.* **86**, 5697–5707 (2012).
41. R. Wang *et al.*, Identification of palmitoyl protein thioesterase 1 in human THP1 monocytes and macrophages and characterization of unique biochemical activities for this enzyme. *Biochemistry* **52**, 7559–7574 (2013).
42. Q. Pan, tRNAome regulating *hepatitis E virus*-triggered inflammasome response, Data *Archiving* and Networked Services (DANS). https://doi.org/10.17026/dans-zyb-9pcv. Deposited 4 May 2023.

Supporting information to

Hepatitis E virus infection remodels the mature tRNAome in macrophages to orchestrate NLRP3 inflammasome response

Yunlong Li[1,2#], Ruyi Zhang[2#], Yining Wang[2], Pengfei Li[2], Yang Li[2], Harry L. A. Janssen[2,3], Robert A. de Man[2], Maikel P. Peppelenbosch[2], Xumin Ou[4,5]*, Qiuwei Pan[2]*

- Materials and Methods
- Supplementary Tables (three)
- Supplementary Figures (twelve)
- References

Supplementary Materials and Methods

Quantification of HEV genome copy numbers

HEV particle copy numbers quantification was performed according to previously described protocols (1). Plasmids containing HEV full-length genome were used as templates for quantifying HEV genome copy numbers. A series of dilutions of plasmid from 10^{-1} to 10^{-9}, were prepared and then were amplified and quantified by qRT-PCR to generate a standard curve. A standard curve was generated by plotting the log copy number versus the cycle threshold (CT) value.

Transfection of HEV RNA

According to previous studies, THP-1 cells can only be transfected before differentiation (2-5). Here, 2.5×10^5 THP-1 cells per well were seeded into 24-well plates and transfected with 300 ng full-length HEV p6 RNA or HEV RNA with GAD mutation (replication-defective) by FuGENE® HD Transfection reagent according to the manufacturer's instructions. Subsequently, 15 ng/mL PMA was added for macrophage differentiation 4 hours after transfection, and after 48 hours supernatant and cells were harvested.

Immunoblot analysis

Concentrated lysates were heated at 95°C for 5 minutes. Proteins were subjected to a 10% sodium dodecyl sulfate polyacrylamide gel (SDS-PAGE), separated at 90 V for 120 minutes, and electrophoretically transferred onto a PVDF membrane (pore size: 0.45 μm; Thermo Fisher Scientific Life Sciences) for 120 minutes with an electric current of 250 mA. Subsequently, the membrane was blocked with blocking buffer (Li-Cor Biosciences). Membranes were incubated with primary antibodies overnight at 4°C. The membrane was washed 3 times, followed by incubation for 1 hour with anti-rabbit or anti-mouse IRDye-conjugated secondary antibodies (1:5000; Li-Cor Biosciences) at room temperature. After washing 3 times, protein bands were detected with Odyssey 3.0 software.

Concentrated supernatants were heated at 95°C for 5 minutes. Proteins were subjected to a 15% sodium dodecyl sulfate polyacrylamide gel (SDS-PAGE), separated at 90 V for 120 min, and electrophoretically transferred onto a PVDF membrane (pore size: 0.45 μm; Thermo Fisher

Scientific Life Sciences) for 120 minutes with an electric current of 250 mA. Subsequently, the membrane was blocked with blocking buffer (Immobilon® Block-Chemiluminescent Blocker, Merck Millipore). Membranes were incubated with primary antibodies overnight at 4°C. The membrane was washed 3 times, followed by incubation for 1 hour with goat anti-rabbit HRP concentration or rabbit anti-mouse HRP concentration (1:10 000; Agilent Technologies Netherlands BV) at room temperature. After washing 3 times, protein bands were incubated with ECL mix for 5 minutes and then detected with AI600 software.

Immunofluorescence staining

3×10^5 THP-1 cells per well were seeded into μ-Slide 8 Well (ibidi GmbH, 80826) and differentiated as previously described, subsequently, cultured for 48 hours with or without HEV incubation. Then cells were fixed with 4% (w/v) paraformaldehyde (PFA) for 10 minutes at room temperature. The well plate with cells was then rinsed 3 times with PBS for 5 minutes each time, followed by permeabilizing with PBS containing 0.2% (vol/vol) tritonX100 for 5 minutes. Then the plates were twice rinsed with PBS for 5 minutes, followed by incubation with blocking solution (5% donkey serum, 1% bovine serum albumin, 0.2% tritonX100 in PBS) at room temperature for 1 hour. Next, plates were incubated in a humidity chamber with primary antibody diluted in blocking solution at 4°C overnight. Primary antibodies used in this study are as follows: ORF2-specific rabbit hyperimmune serum (1:250, rabbit), anti-dsRNA antibody (1:500, mouse mAb). Excess primary antibodies were removed and the plates were washed 3 times for 5 min each in PBS prior to 1 hour incubation with 1:1000 dilutions of the anti-mouse IgG (H + L, Alexa Fluor® 594), the anti-rabbit IgG (H + L, Alexa Fluor® 488) secondary antibodies at room temperature. Nuclei were stained with DAPI (4, 6-diamidino-2-phenylindole; Invitrogen). The fluorescence was assayed by Leica sp5 confocal microscope with a 40 × oil immersion objective.

MTT assay

Cells were seeded in 96-well plates (5×10^4 per well) and differentiated as described. Then treated according to experimental requirements and cultured for 12, 24, or 48 hours and 10mM 3-(4,5-dimethylthiazol-2-yl)-2,5-diphenyltetrazolium bromide (MTT) (Sigma-Aldrich) was added. The plate was incubated at 37°C with 5% CO2 for 3 hours, then the medium was removed, and

100 μL of DMSO was added to each well. The plate was incubated at 37°C for 1 hour. The absorbance was read on the microplate absorbance reader (Bio-Rad, Hercules, CA, USA) at a wavelength of 490 nm.

Enzyme-linked immunosorbent assay (ELISA)

The concentrations of IL-1β in cell culture supernatant were measured by the ELISA Kit (BD Biosciences, San Jose, CA, USA) according to the manufacturer's instructions.

Supplementary tables

Supplementary Table 1. Experimental resource.

REAGENT or RESOURCE	SOURCE	IDENTIFIER
Antibodies		
IL-1β (D3U3E) antibody, Rabbit mAb	Cell Signaling Technology	Cat# 12703
Cleaved IL-1β (Asp116) (D3A3Z)	Cell Signaling Technology	Cat# 83186s
Cleaved Caspase-1 (Asp297) (D57A2)	Cell Signaling Technology	Cat# 4199s
NF-κB p65 (D14E12) XP® Rabbit mAb	Cell Signaling Technology	Cat# 8242
Phospho-NF-κB p65 (Ser536) (93H1) Rabbit mAb	Cell Signaling Technology	Cat# 3033
anti-dsRNA mAb J2	SCICONS	Cat# 10010200
HEV, MS x 1E6	Sigma-Aldrich Chemie BV	Cat#: MAB8002
ORF2-specific rabbit hyperimmune serum	Group R. Ullrich, Friedrich Loeffler Institute, Germany	N/A
β-actin antibody, mouse mAb	Santa Cruz Biotechnology	Cat# sc-47778
IRDye® 680RD Goat anti-Mouse IgG (H + L)	Westburg BV	Cat# 926-68070; RRID: AB_10956588
IRDye® 800CW Goat anti-Rabbit IgG (H + L)	Westburg BV	Cat# 926-32211; RRID: AB_621843
Gt a Rabbit Immunoglobulins/HRP (1 mL)	Agilent Technologies Netherlands BV	Cat# P044801-2
Rb a Mo Immunoglobulins/HRP (2 mL)	Agilent Technologies Netherlands BV	Cat# P026002-2
NLRP3 Antibody, rabbit pAb	ThermoFisher Scientific	Cat# PA5-20838; RRID: AB_11154455
Virus strains		
HEV, Kernow-C1 p6 clone, JQ679013	S. U. Emerson et al.	N/A
Chemicals		
Immobilon® Block - FL (Fluorescent Blocker)	Merck Chemicals BV	Cat# WBAVDFL01
Intercept® (PBS) Blocking Buffer	LI-COR	Cat# 927-70010
Immobilon-FL PVDF, 0.45 µm, 8.5 cm x 10 m roll	Merck Chemicals BV	Cat# IPFL85R
PrimeScript™ RT Master Mix (Perfect Real Time)	Takara Bio Europe S.A.S.	Cat# RR036A
MicroAmp Fast Optical 96-Well Reaction Plate	Life Technologies Europe BV	Cat# 4346907
SYBR Select Master Mix for CFX-10 x 5 mL	Fisher Scientific	Cat# 4472954
Immobilon ECL Ultra Western HRP Substrate	Merck Chemicals BV	Cat# WBULS0100
Thiazolyl blue tetrazolium bromide (MTT)	Sigma-Aldrich Chemie BV	Cat# M2128-5G
12-O-Tetradecanoylphorbol 13-acetate (PMA)	Sigma-Aldrich Chemie BV	Cat# P1585-1MG
ATP (Adenosine 5'-triphosphate)	MedChemExpress	Cat# HY-B2176
T4 RNA Ligase 2 (dsRNA Ligase)	Bioké	Cat# M0239L
RPL22 RPMI 1640-Liquid without amino acids	Caisson Labs	Cat# 11211009
RPMI 1640 medium	ThermoFisher Scientific	Cat# 11875093

L-GLUTAMINE, BIOULTRA, >= 99.5 % NT	Sigma-Aldrich	Cat# 49419-25G
L-GLUTAMIC ACID, REAGENTPLUS(TM), >=99%&	Sigma-Aldrich	Cat# G1251-100G
GLYCINE, BIOULTRA, FOR MOLECULAR BIOLOGY	Sigma-Aldrich	Cat# 50046-50G
L-ASPARTIC ACID, BIOXTRA, >=99% (HPLC)	Sigma-Aldrich	Cat# A8949-25G
TRANS-4-HYDROXY-L-PROLINE, 99+%	Sigma-Aldrich	Cat# H54409-2.5G
L-LYSINE MONOHYDROCHLORIDE MEETS EP, JP&	Sigma-Aldrich	Cat# L8662-25G
FuGENE® HD Transfection reagent	Promega	Cat# E2311
L-Arginine	Bio-Connect BV	Cat# 0219462725
L-Proline	Sigma-Aldrich	Cat# P5607-25G
L-Histidine	Sigma-Aldrich	Cat# H8000-5G
L-Isoleucine	Sigma-Aldrich	Cat# I2752-1G
L-Leucine	Sigma-Aldrich	Cat# L8000-25G
L-Methionine	Sigma-Aldrich	Cat# M9625-5G
L-Phenylalanine	Sigma-Aldrich	Cat# P5482-25G
L-Serine	Sigma-Aldrich	Cat# S4500-1G
L-Threonine	Sigma-Aldrich	Cat# T8625-1G
L-Tryptophan	Sigma-Aldrich	Cat# T0254-1G
L-Tyrosine	Sigma-Aldrich	Cat# T8566-25G
L-Valine	Sigma-Aldrich	Cat# V0500-1G
L-Asparagine	Sigma-Aldrich	Cat# A4159-25G
L-Cystine	Sigma-Aldrich	Cat# C7602-10MG
Lipopolysaccharide (LPS)	Sigma-Aldrich	Cat# L6529
BAY11 7085	Santa Cruz Biotech	Cat# sc-202490
MCC950	Invivogen	Cat# inh-mcc
Belnacasan (VX-765)	Bio-Connect BV	Cat# S2228
Critical commercial assays		
Human IL-1 beta/IL-1F2 Quantikine ELISA Kit	Bio-Techne	Cat# DLB50
Macherey NucleoSpin RNA II Kit	Bioke	Cat# 740955.250
Experimental models: Cell lines		
THP-1	Erasmus University Medical Center	N/A
HL 60	Erasmus University Medical Center	N/A
Software and algorithms		
Relative Synonymous Codon Usage (RSCU) analysis	D. Paulet and A. David, E (6)	N/A

Supplementary Table 2. Primer sequences

Gene	Sequence (5'-3')
HEV sense	GGTGGTTTCTGGGGTGAC
HEV anti sense	AGGGGTTGGTTGGATGAA
GAPDH sense	GTCTCCTCTGACTTCAACAGCG
GAPDH anti sense	ACCACCCTGTTGCTGTAGCCAA
CD11B-Human sense	GAACCAGCCCAGAGGTGACTG
CD11B-Human anti sense	GGATGACAAACGACTGCTCCTG
CD68-Human sense	ACCTCGACCTGCTCTCCCTG
CD68-Human anti sense	CGAGGAGGCCAAGAAGGATC
IL-1β sense	CCACAGACCTTCCAGGAGAATG
IL-1β anti sense	GTGCAGTTCAGTGATCGTACAGG
IL-6 sense	AGACAGCCACTCACCTCTTCAG
IL-6 anti sense	TTCTGCCAGTGCCTCTTTGCTG
IL-8 sense	GAGAGTGATTGAGAGTGGACCAC
IL-8 anti sense	CACAACCCTCTGCACCCAGTTT
IL-12 sense	GACATTCTGCGTTCAGGTCCAG
IL-12 anti sense	CATTTTTGCGGCAGATGACCGTG
IL-18 sense	GATAGCCAGCCTAGAGGTATGG
IL-18 anti sense	CCTTGATGTTATCAGGAGGATTCA
TNF α sense	CTCTTCTGCCTGCTGCACTTTG
TNF α anti sense	ATGGGCTACAGGCTTGTCACTC
GM-CSF sense	GGAGCATGTGAATGCCATCCAG
GM-CSF anti sense	CTGGAGGTCAAACATTTCTGAGAT

Supplementary Table 3. shRNA sequences.

ID	Symbol	TargetTaxonId	TargetSeq	GeneDesc	OligoSeq
1[#]	LARS	Human	GCTAACTATTAAG GAGGATAA	leucyl-tRNA synthetase	CCGGGCTAACTATTAAGGA GGATAACTCGAGTTATCCT CCTTAATAGTTAGCTTTTTG
2[#]	LARS	Human	GCTGTGCTTATGG AGAATATA	leucyl-tRNA synthetase	CCGGGCTGTGCTTATGGAG AATATACTCGAGTATATTCT CCATAAGCACAGCTTTTTG
3[#]	LARS	Human	CGCTCCATTCTGT CCACATTT	leucyl-tRNA synthetase	CCGGCGCTCCATTCTGTCC ACATTTCTCGAGAAATGTGG ACAGAATGGAGCGTTTTTG
4[#]	LARS	Human	CCTCACTTTGACC CAAGCTAT	leucyl-tRNA synthetase	CCGGCCTCACTTTGACCCAA GCTATCTCGAGATAGCTTGG GTCAAAGTGAGGTTTTTG

Supplementary figures

A

B

C

D
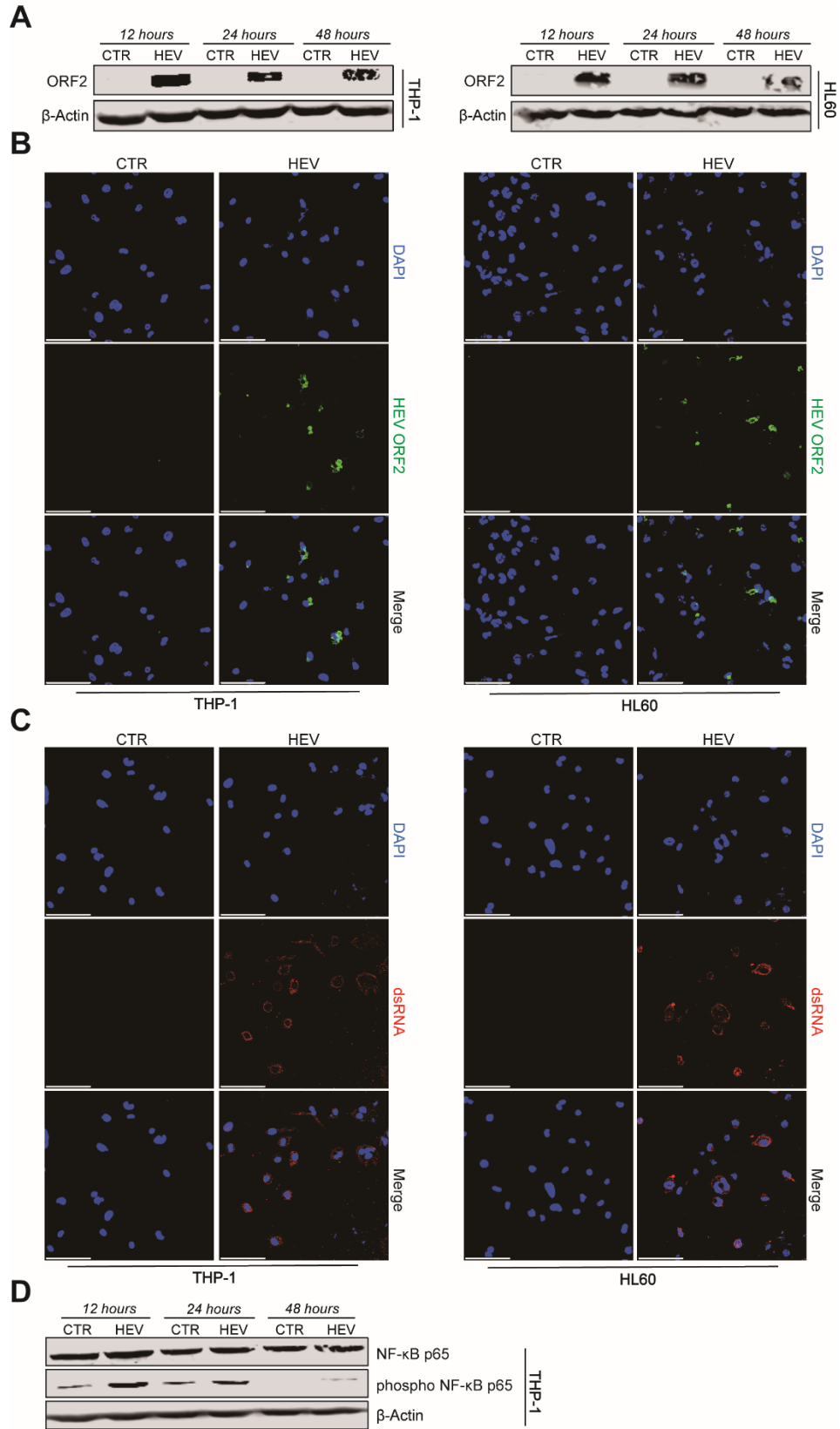
Figure S1. Differentiated THP-1 and HL60 macrophages support HEV infection, related to Figure 1. THP-1 and HL60 macrophages were inoculated with HEV and viral protein levels were detected by western blotting **(A)**. Immunofluorescence analysis of viral ORF2-encoded capsid protein **(B)**, or viral double-strand RNA (dsRNA) **(C)** was performed 48 hours after HEV inoculation. Uninfected THP-1 or HL60 cells incubated with the anti-HEV capsid protein antibody or anti-dsRNA antibody serves as the negative control. DAPI (blue) was applied to visualize nuclei (Scale bar, 100 μm. 40× oil immersion objective). **(D)** THP-1 macrophages were inoculated with HEV for 12, 24, or 48 hours. NF-κB p65 and phosphor NF-κB p65 were determined by western blotting.
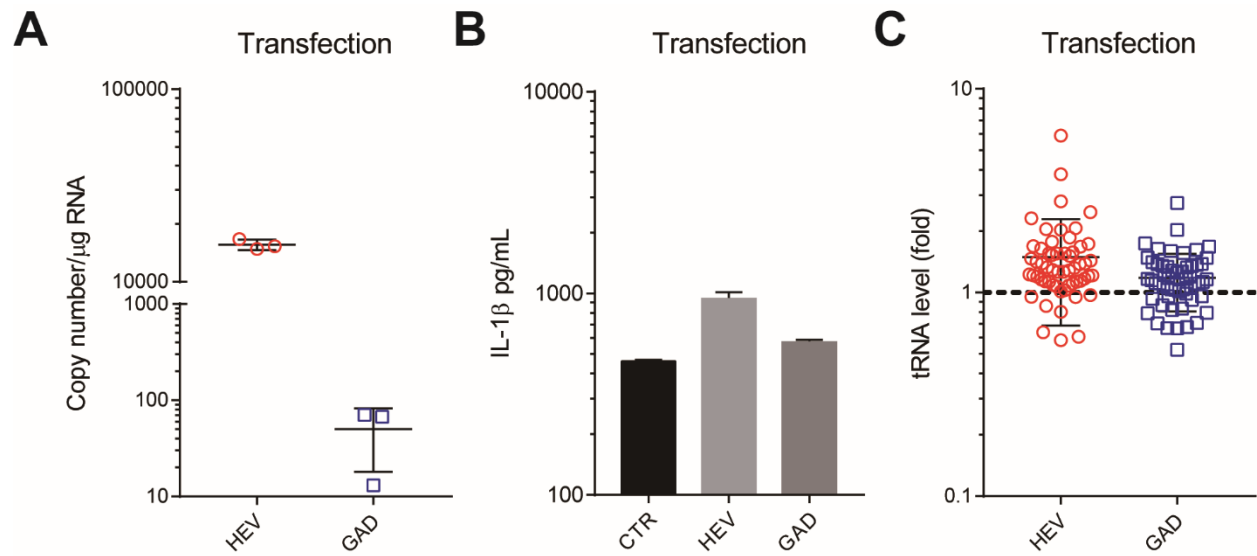
Figure S2. Transfection of HEV genomic RNA provokes tRNAome remolding, related to Figure 1. THP-1 cells transfected with 300 ng full-length HEV p6 RNA or HEV GAD mutation RNA (replication-defective) for 48 hours. The HEV copy numbers were quantified by qRT-PCR (n = 3) **(A)**, IL-1β protein secretion was quantified by ELISA (n = 4) **(B)**. **(C)** Accordingly, the mature tRNAome consisting of 57 species was quantified by qRT-PCR. Data were normalized to the control (CTR; set as 1). Data are means ± SEM.
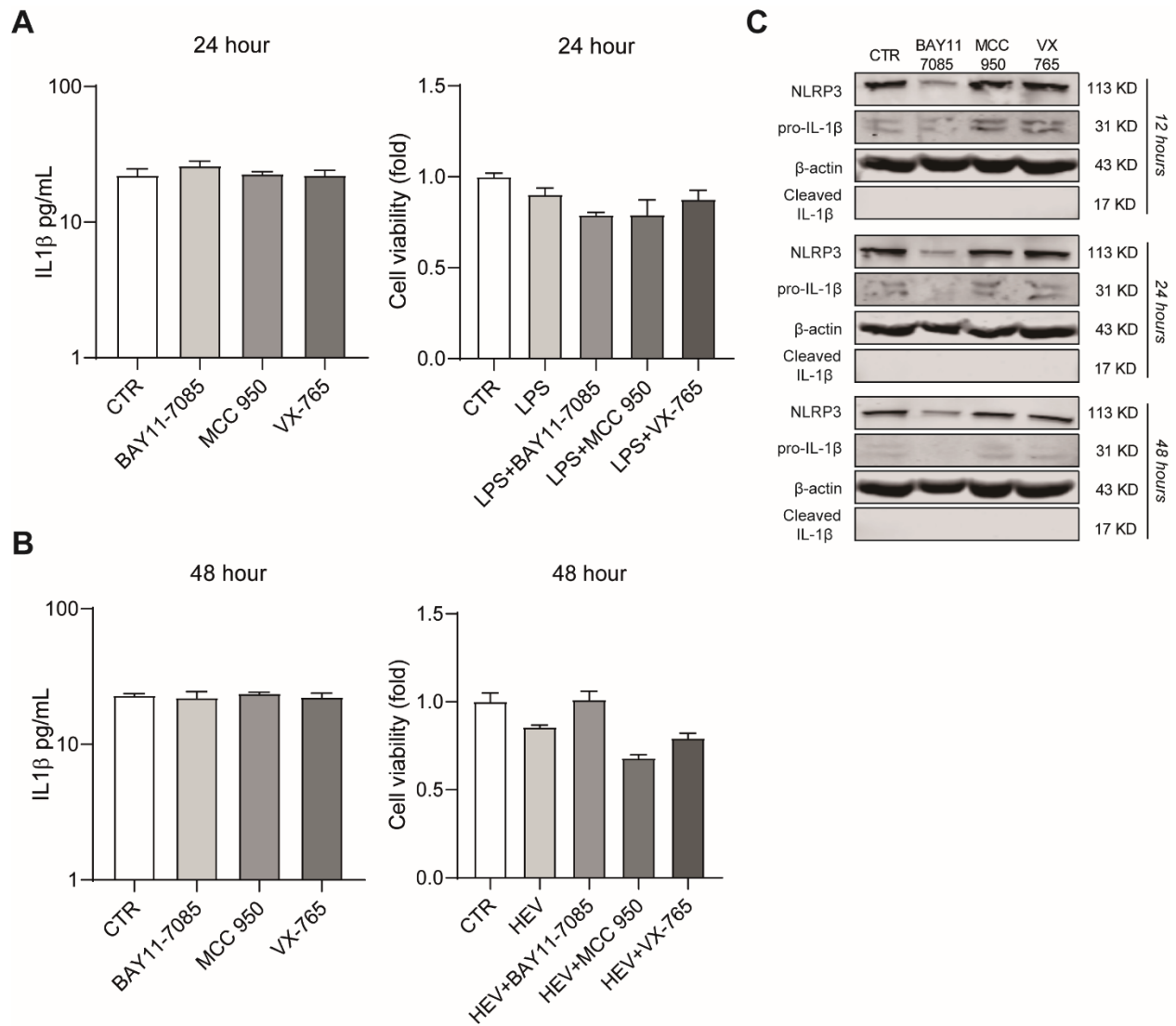
Figure S3. BAY11 7085, MCC950, and VX-765 treatment on the basal level of IL-1β secretion, cell viability, and NLRP3 inflammasome response, related to Figure 2. (A) Quantitative analysis of IL-1β secretion in THP-1 macrophages without HEV infection by ELISA after 10 µM BAY11-7085, 10 µM MCC950, or 50 µM VX-765 for 24 hours (n = 4). MTT assay analysis of cell viability in THP-1 macrophages treated with LPS or LPS plus 10 µM BAY11-7085, 10 µM MCC950, or 50 µM VX-765 for 24 hours (n = 6). **(B)** Quantitative analysis of IL-1β secretion THP-1 macrophages without HEV infection by ELISA after 10 µM BAY11-7085, 10 µM MCC950, or 50 µM VX-765 for 48 hours (n = 4). MTT assay analysis of cell viability in THP-1 macrophages infected with HEV or HEV plus 10 µM BAY11-7085, 10 µM MCC950, or 50 µM VX-765 for 48 hours (n = 6). Data are means ± SEM. **(C)** THP-1 macrophages without HEV infection were treated with 10 µM BAY11-7085, 10 µM MCC950, or 50 µM VX-765 for 12, 24, or 48 hours. Mature IL-1 β in supernatant or pro-IL-1β and NLRP3 in lysates were determined by western blotting.
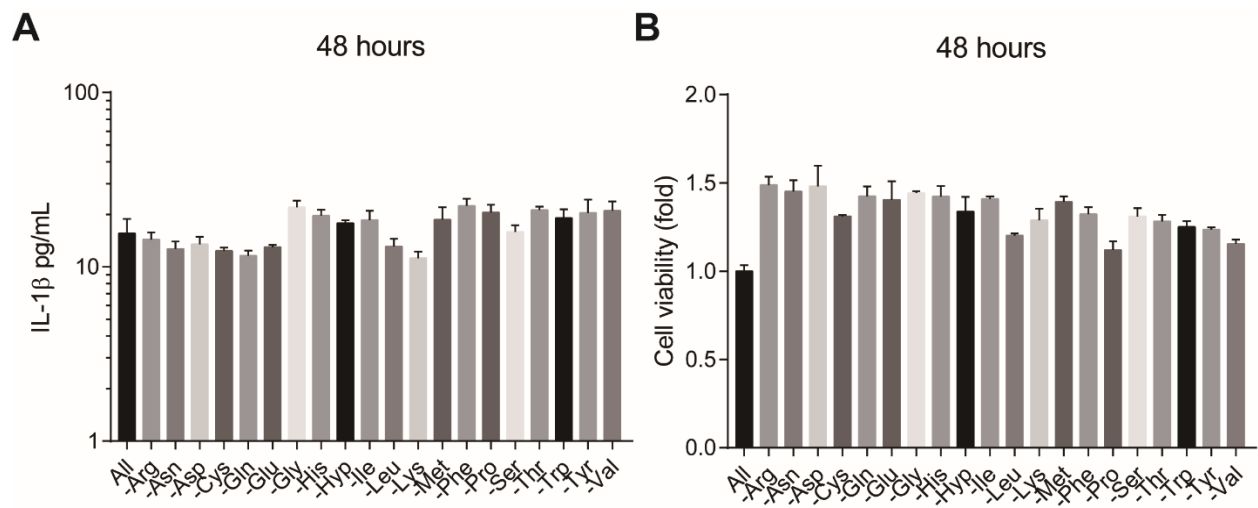
Figure S4. The effect of amino acid deprivation on IL-1β secretion and cell viability, related to Figure 3. THP-1 macrophages without HEV infection were cultured in medium containing 20 amino acids for 48 hours. **(A)** Quantitative analysis of IL-1β secretion by ELISA (n = 4). **(B)** MTT assay analysis of cell viability (n = 4).
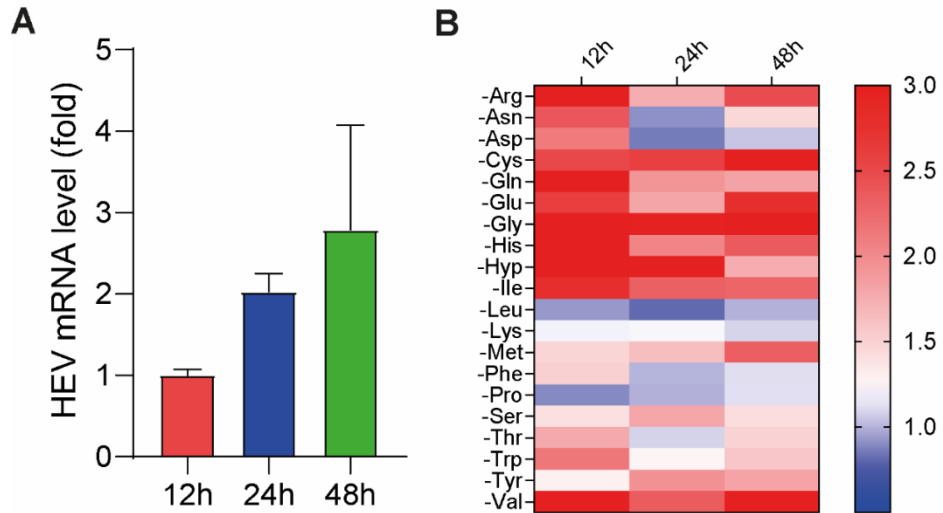
Figure S5. The effect of amino acid deprivation on HEV replication, related to Figure 3. (A) THP-1 macrophages were cultured in medium containing 20 amino acids and inoculated with HEV and viral RNA levels were quantified by qRT-PCR (n = 3). The group with HEV infection for 12 hours was set as 1. **(B)** THP-1 macrophages were subjected to the deprivation of each of the 20 amino acids in RPMI 1640 and inoculated with HEV. The HEV viral RNA levels were quantified by qRT-PCR, and data were normalized to the non-amino acid deprivation group (set as 1). Data are means ± SEM.
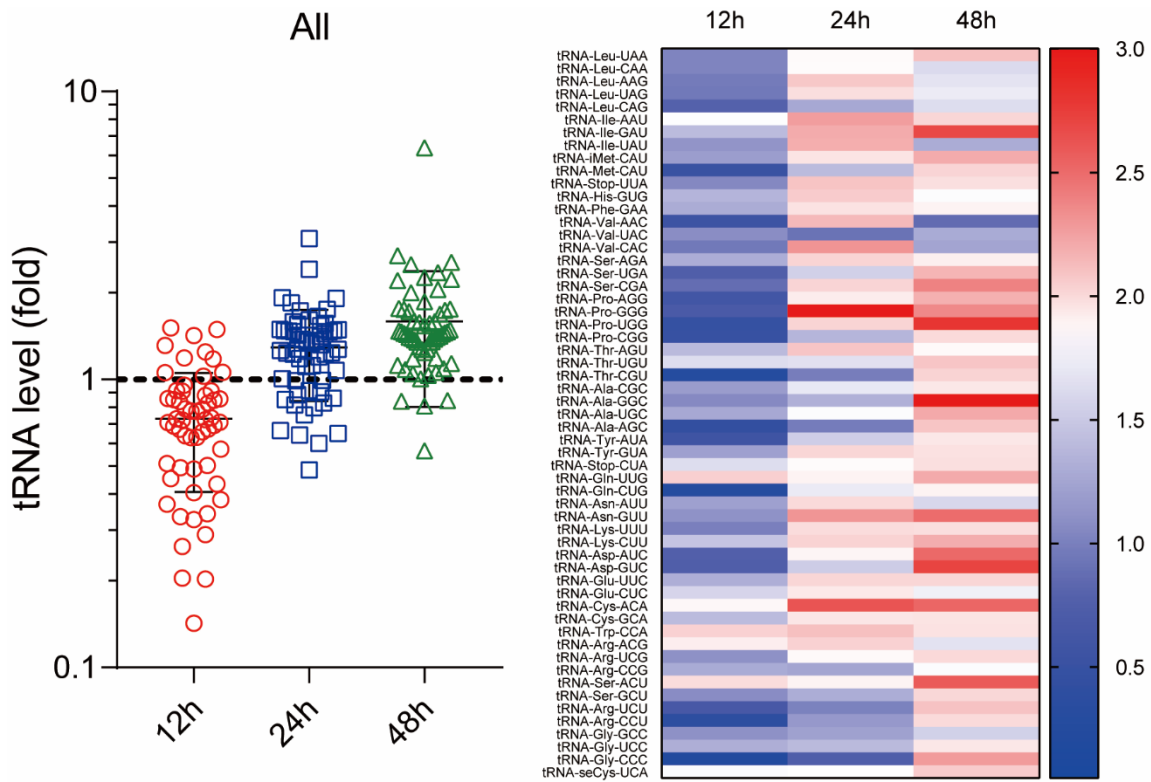
Figure S6. The control medium without amino acid deprivation does not affect HEV-provoked tRNAome remodeling, related to Figure 3. THP-1 macrophages were subjected to 20 amino acid-containing RPMI 1640 medium and inoculated with HEV for 12, 24, or 48 hours. The mature tRNAome was quantified by qRT-PCR, and data were normalized to the uninfected control (CTR; set as 1).
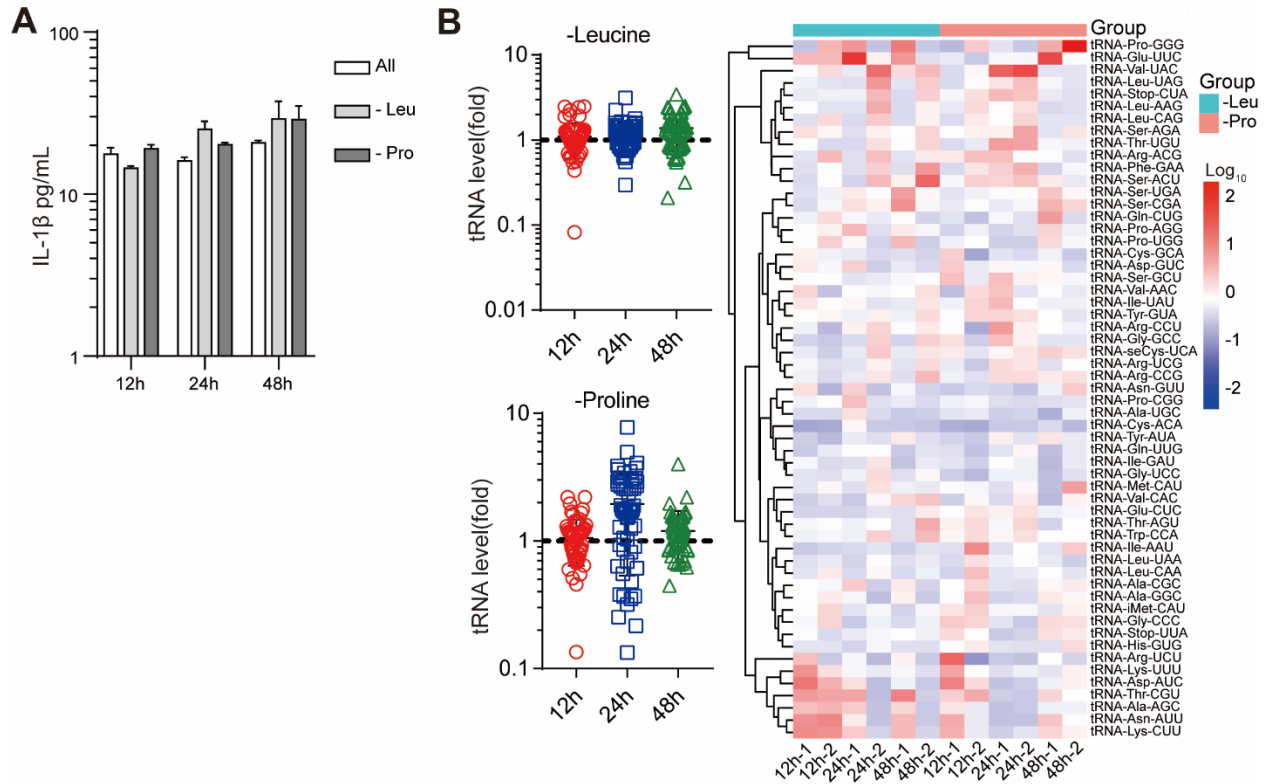
Figure S7. Leucine or proline deprivation does not affect IL-1β secretion and mature tRNAome expression at basal level, related to Figure 4. THP-1 macrophages without HEV infection were subjected to 20 amino acid-containing, leucine deprivation, or proline deprivation RPMI 1640 medium and cultured for 12, 24, or 48 hours. **(A)** IL-1β protein levels were quantified by ELISA (n = 4). **(B)** The mature tRNAome was quantified by qRT-PCR. Cluster analysis of the tRNAome and data were normalized to the non-amino acids deprivation control (CTR; set as 1). Data are means ± SEM.
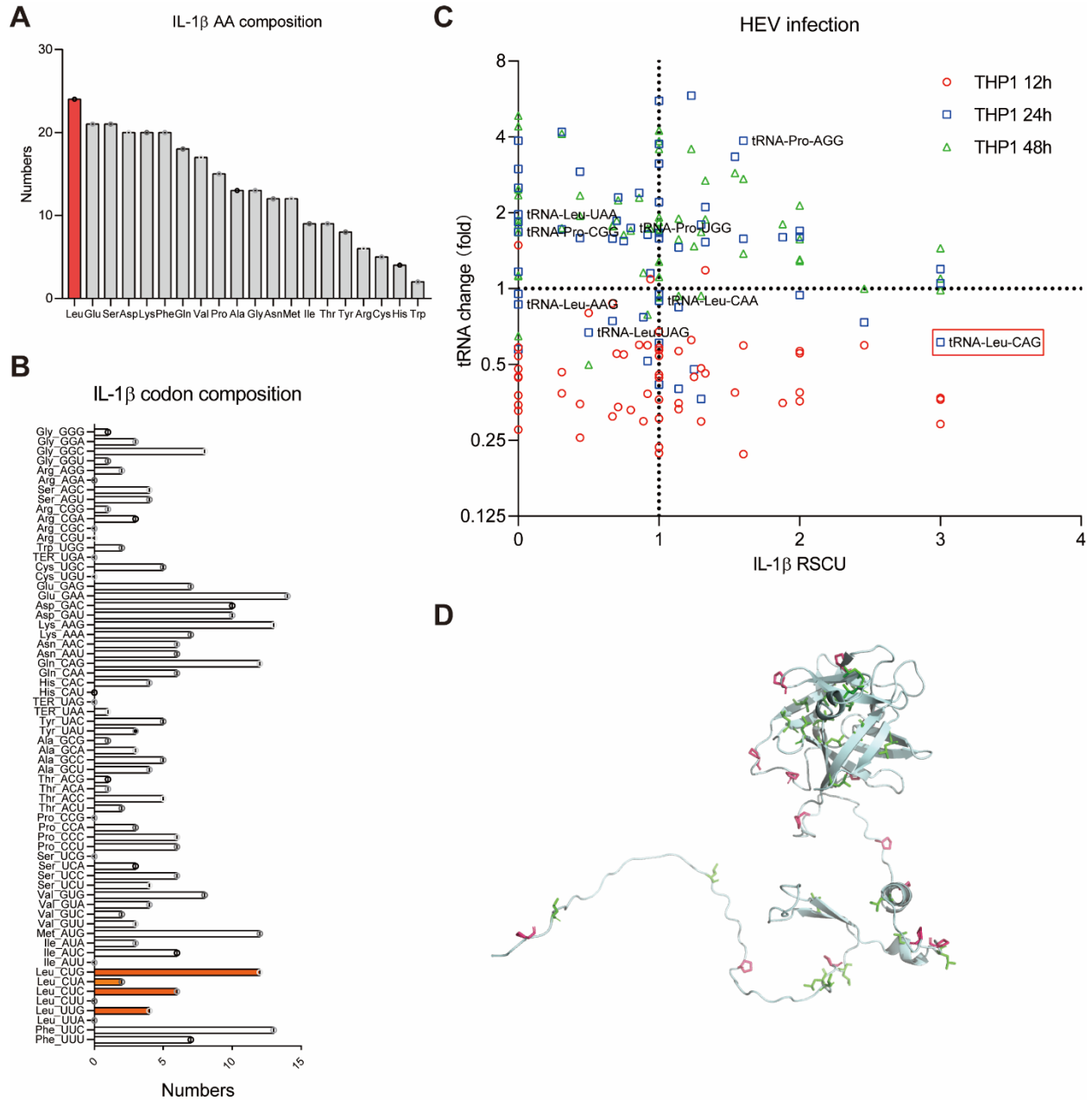
Figure S8. The relation of tRNAome landscape and IL-1β, related to Figure 4. (A) The amino acid composition of IL-1β protein. **(B)** The codon composition analysis according to the IL-1β mRNA sequence. **(C)** THP-1 macrophages were inoculated with HEV for 12, 24, or 48 hours. Mature tRNAome were quantified by qRT-PCR and then Relative Synonymous Codon Usage (RSCU) analysis was performed. **(D)** IL-1β protein structure analysis. The green color is leucine and the red color is proline. Data are means ± SEM.
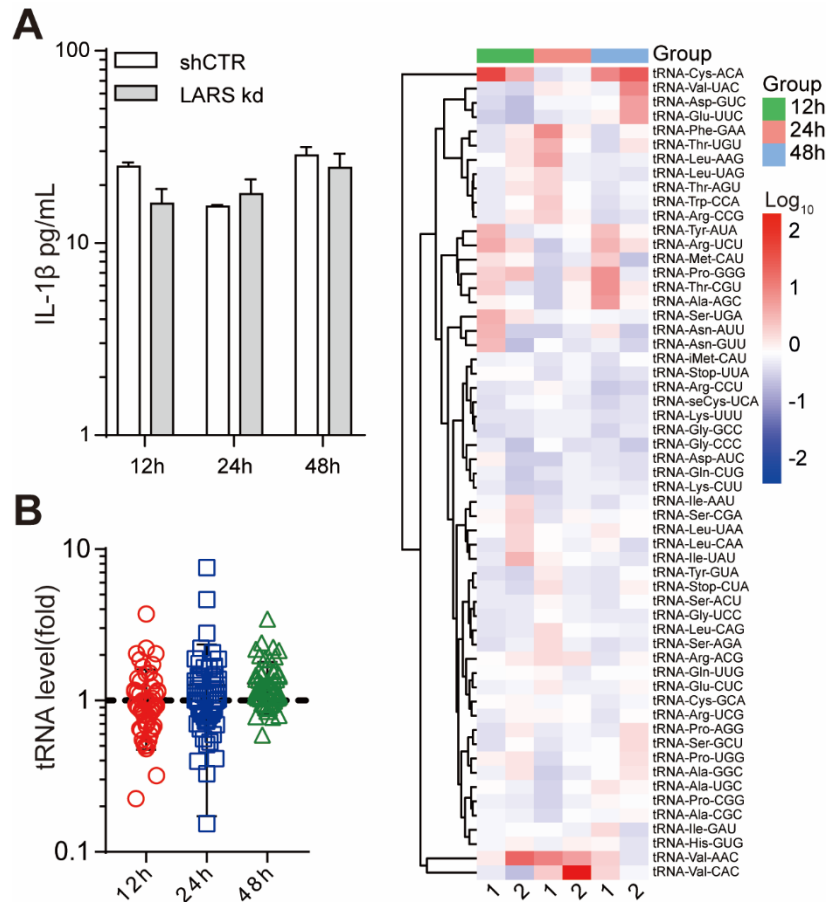
Figure S9. The basal levels of IL-1β secretion and mature tRNAome expression in the THP-1 LARS knockdown cell line without HEV infection, related to Figure 5. Effects of LARS knockdown on IL-1β secretion and mature tRNAome expression measured after cultured 12, 24, or 48 hours. **(A)** IL-1β protein levels were quantified by ELISA (n = 4). **(B)** The mature tRNAome was quantified by qRT-PCR. Cluster analysis of the tRNAome and data were normalized to the shCTR (CTR; set as 1). Data are means ± SEM.
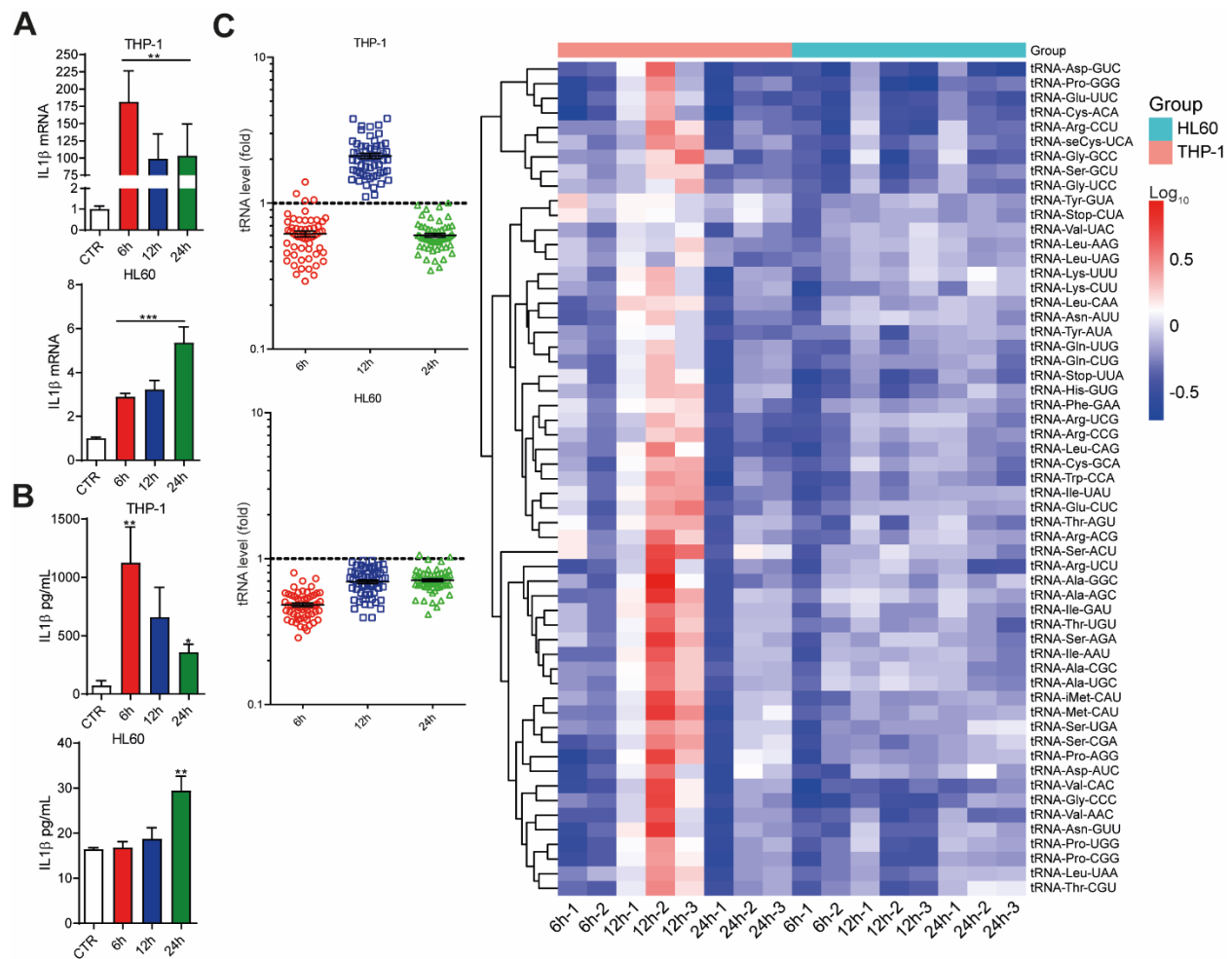
Figure S10. IL-1β expression and the mature tRNAome landscape after LPS treatment. THP-1 and HL60 macrophages were treated with LPS (400 ng/mL) for 6, 12, or 24 hours, followed by ATP (5 mM) for 40 minutes. IL-1β mRNA (**A**) and protein (**B**) levels were quantified by qRT-PCR (n = 6-7) and ELISA (n = 5), respectively. **(C)** THP-1 and HL60 macrophages were treated with LPS (400 ng/mL) for 6, 12, or 24 hours, followed by ATP (5 mM) for 40 minutes. The mature tRNAome consisting of 57 species was quantified by qRT-PCR. Cluster analysis of the tRNAome and data were normalized to the untreated control (CTR; set as 1). Data are means ± SEM. *p < 0.05; **p < 0.01; ***p < 0.001.
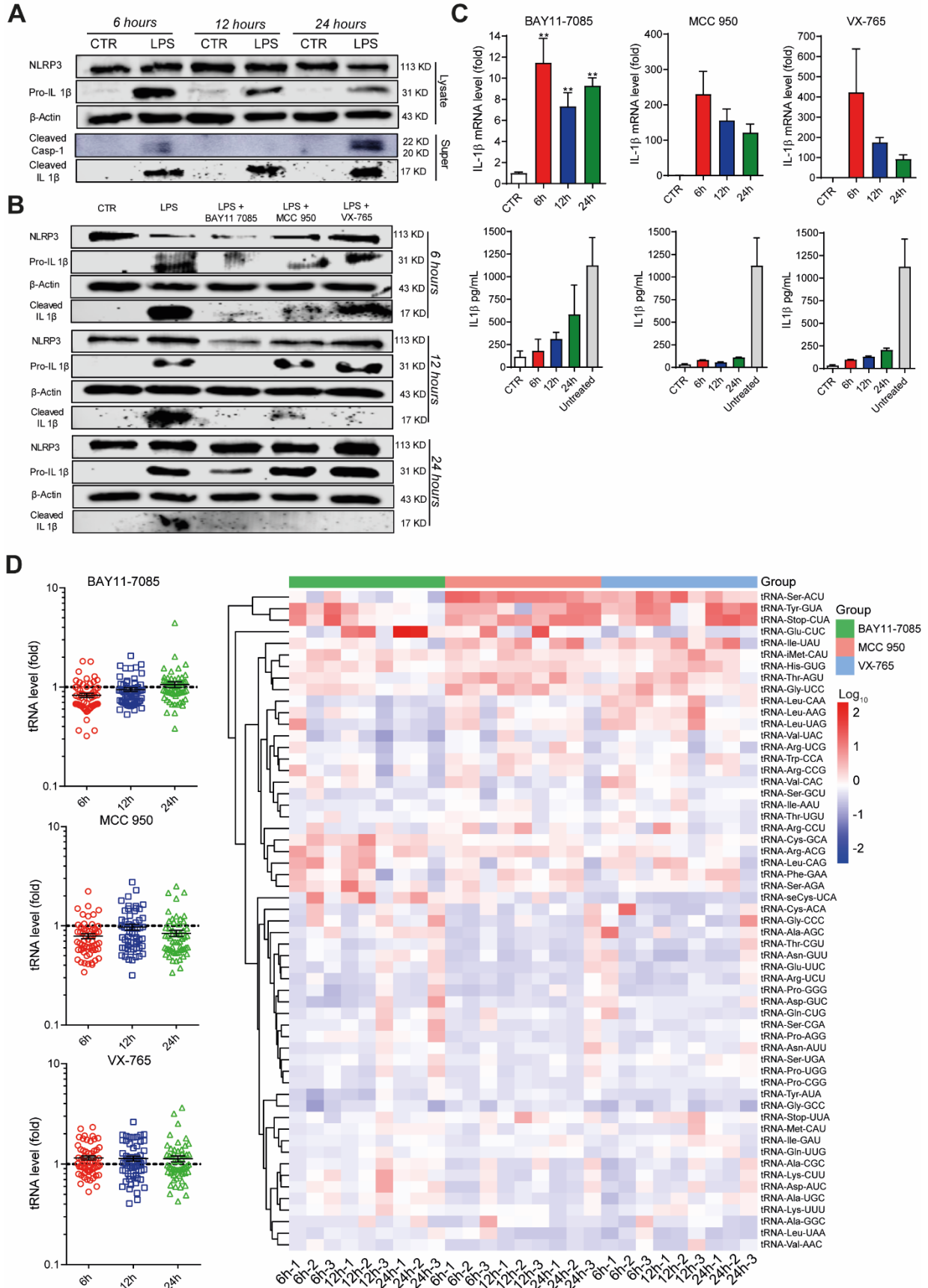
Figure S11. Inhibition of NLRP3 inflammasome prevents LPS-induced tRNAome remodeling. (A) THP-1 macrophages were treated with LPS (400 ng/mL) for 6, 12, or 24 hours, followed by ATP (5 mM) for 40 minutes. Mature IL-1β and cleaved caspase-1 in supernatant or pro-IL-1β and NLRP3 in lysates were determined by western blotting. THP-1 macrophages were pretreated with 10 μM NF-κB inhibitor (BAY11-7085), 10 μM NLRP3 inhibitor (MCC950), or 50 μM caspase-1 inhibitor (VX-765) for 2 hours and then were treated with LPS (400 ng/mL) or LPS (400 ng/mL) plus 10 μM BAY11-7085, 10 μM MCC950, or 50 μM VX-765 for 6, 12, or 24 hours, followed by ATP (5 mM) for 40 minutes. **(B)** Mature IL-1β in supernatant or pro-IL-1β and NLRP3 in lysates were determined by western blotting. **(C)** IL-1β mRNA and protein levels were quantified by qRT-PCR (n = 3-6) and ELISA (n = 4), respectively. **(D)** The mature tRNAome was quantified by qRT-PCR. Cluster analysis of the tRNAome and data were normalized to the control (CTR; set as 1). Data are means ± SEM. *p < 0.05; **p < 0.01.
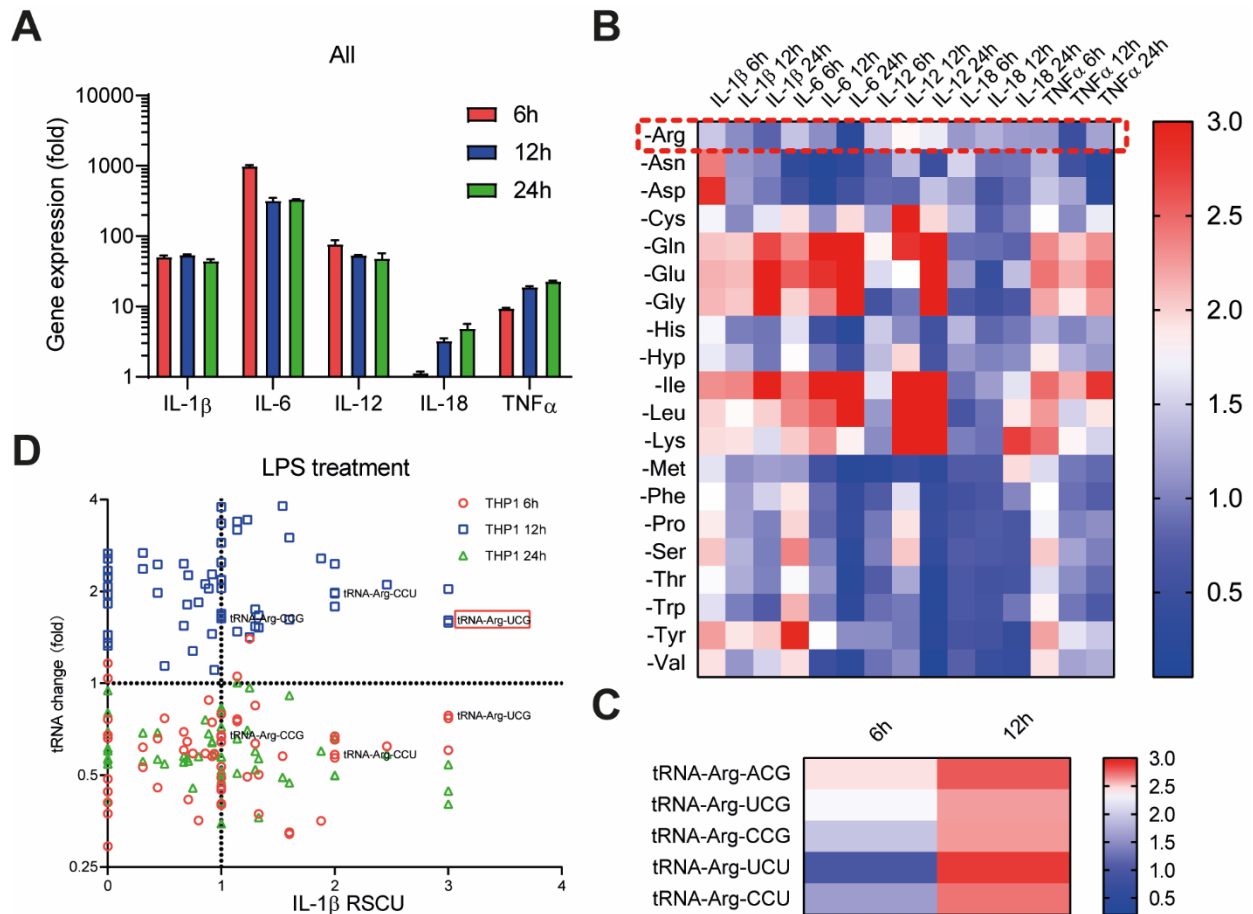
Figure S12. Amino acid deprivation affects LPS treatment-induced inflammatory gene expression. (A) THP-1 macrophages were cultured in medium containing 20 amino acids and treated with LPS (400 ng/mL) for 6, 12, or 24 hours, followed by ATP (5 mM) for 40 minutes. Gene expression of IL-1β, IL-6, IL-8, IL-12, TNFα, and GM-CSF was quantified by qRT-PCR (n = 2). **(B)** THP-1 macrophages were subjected to the deprivation of each of the 20 amino acids in RPMI 1640 and treated with LPS (400 ng/mL) for 6, 12, or 24 hours, followed by ATP (5 mM) for 40 minutes. The expression of inflammatory genes was quantified by qRT-PCR (n = 3), and data were normalized to the non-amino acid deprivation group (set as 1). **(C)** THP-1 macrophages were treated with LPS (400 ng/mL) for 6 or 12hours, followed by ATP (5 mM) for 40 minutes. The cognate tRNAs of arginine were quantified by qRT-PCR (n = 2-3), and data were normalized to the treated group (set as 1). **(D)** THP-1 macrophages were treated with LPS (400 ng/mL) for 6, 12, or 24 hours, followed by ATP (5 mM) for 40 minutes. Mature tRNAs were quantified by qRT-PCR and then Relative Synonymous Codon Usage (RSCU) analysis was performed. Data are means ± SEM.

References

1. Li P*, et al.* (2022) Recapitulating hepatitis E virus-host interactions and facilitating antiviral drug discovery in human liver-derived organoids. *Science advances* 8(3):eabj5908.
2. Maeß MB, Wittig B, Cignarella A, & Lorkowski S (2014) Reduced PMA enhances the responsiveness of transfected THP-1 macrophages to polarizing stimuli. *Journal of immunological methods* 402(1-2):76-81.
3. Schnoor M*, et al.* (2009) Efficient non-viral transfection of THP-1 cells. *Journal of immunological methods* 344(2):109-115.
4. Maess MB, Buers I, Robenek H, & Lorkowski S (2011) Improved protocol for efficient nonviral transfection of premature THP-1 macrophages. *Cold Spring Harbor protocols* 2011(5):pdb.prot5612.
5. Tang X*, et al.* (2018) A method for high transfection efficiency in THP-1 suspension cells without PMA treatment. *Analytical biochemistry* 544:93-97.
6. Paulet D, David A, & Rivals E (2017) Ribo-seq enlightens codon usage bias. *DNA research : an international journal for rapid publication of reports on genes and genomes* 24(3):303-210.